THESIS FOR THE DEGREE OF DOCTOR OF PHILOSOPHY

Binary mixtures and cationic modification of protic ionic liquids

Local structure and transport properties

Iqbaal Abdurrokhman

Department of of Chemistry and Chemical Engineering
CHALMERS UNIVERSITY OF TECHNOLOGY
Göteborg, Sweden 2021

Binary mixtures and cationic modification of protic ionic liquids

Local structure and transport properties

Iqbaal Abdurrokhman

ISBN 978-91-7905-550-9

Doktorsavhandlingar vid Chalmers tekniska högskola

Ny serie Nr. 5017

ISSN 0346-718X

Department of of Chemistry and Chemical Engineering
Chalmers University of Technology
SE-412 96 Göteborg
Sweden
Telephone +46 31 772 1000

Cover:
A cartoon illustrating a droplet of protic ionic liquids.

Printed by Chalmers Reproservice
Göteborg, Sweden 2021

Binary mixtures and cationic modification of protic ionic liquids
Local structure and transport properties

Iqbaal Abdurrokhman
Department of of Chemistry and Chemical Engineering
Chalmers University of Technology

Abstract

Protic ionic liquids are a subclass of ionic liquids, which in many cases are obtained by mixing an equimolar amount of Brønsted acid and base. Protic ionic liquids possess an exchangeable proton that gives them distinct features, *e.g.* the potential to conduct protons and the ability to form extended hydrogen bonds, which is different from the case of their aprotic counterparts.

The protic ionic liquids considered in this thesis are limited to those based on the imidazolium and triazolium cation, which (compared to aprotic ionic liquids) are less developed and have been investigated to a lesser extent. The work included in this thesis has been devoted to investigate strategies that could possibly promote a fast proton motion. These strategies have primarily consisted in mixing a protic ionic liquid with a molecular solvent or another parented ionic liquid and in modifying the cationic structure by either attaching alkyl chains of different length to the imidazolium cation or synthesizing new protic ionic liquids derived from another heterocyclic ring such as triazole. In both cases, a detailed characterization by means of vibrational spectroscopy could provide valuable information about intermolecular interactions. An important finding from the studies conducted in this thesis is that altering the cation's structure or adding a co-solvent leads to a significant change in chemical and transport properties.

This thesis also includes an extensive work devoted to develop a new solvent-free method to synthesize dry and pure protic ionic liquids, in the laboratory scale. An analytical approach to accurately quantify their purity using nuclear magnetic spectroscopy has also been developed. In addition, the ionic conductivity of the investigated protic ionic liquid systems has been evaluated by use of impedance spectroscopy, from room temperature up to 140 °C. The results included in my work indicate that the two investigated strategies can potentially be used, each with its limitations, to develop thermochemically stable proton conducting materials based on protic ionic liquids.

Keywords: Protic ionic liquids, binary mixtures, proton mobility, cationic modification, synthesis, imidazolium, triazolium, vibrational spectroscopy, nuclear magnetic spectroscopy, impedance spectroscopy

List of Publications

This thesis is based on the following appended papers:

I. Transport properties and intermolecular interactions in binary mixtures based on the protic ionic liquid ethylimidazolium triflate and ethylene glycol

Negin Yaghini, Iqbaal Abdurrokhman, Mohammad Hasani and Anna Martinelli

Physical Chemistry Chemical Physics **(2018)**, Vol. 20 (35), 22980–22986

II. Protic Ionic Liquids Based on the Alkyl-Imidazolium Cation: Effect of the Alkyl Chain Length on Structure and Dynamics

Iqbaal Abdurrokhman, Khalid Elamin, Olesia Danyliv, Mohammad Hasani and Anna Martinelli

Journal of Physical Chemistry B **(2019)**, Vol. 123 (18), 4044–4054

III. Solvent-free synthesis of protic ionic liquids. Synthesis, characterization, and computational studies of triazolium based ionic liquids

Eduardo Maurina Morais‡, Iqbaal Abdurrokhman‡ and Anna Martinelli

Submitted to Journal of Molecular Liquids **(2021)**

IV. Binary mixtures of imidazolium based protic ionic liquids. Phase behaviour, ionic conductivity and vibrational spectra

Iqbaal Abdurrokhman and Anna Martinelli

Manuscript **(2021)**

My Contributions to the Publications

Paper I

Responsible for collecting and analysing the vibrational spectroscopic data, wrote the corresponding section and discussed with other authors all the results to finalise the article.

Paper II

Responsible for most of the experimental work, the interpretation of the experimental results, writing the first draft of the article, and contributing actively to the overall editing process of the article. With the exception for the X-ray scattering experiments, which were performed by Olesia Danyliv, and the diffusion NMR measurements, which were performed by Mohammad Hasani.

Paper III

‡ Equal contribution. Iqbaal Abdurrokhman and Eduardo M. Morais have together designed and performed all the experiments. In addition, E.M.M carried out the computational experiments. I.A. and E.M.M. have processed the experimental data, performed the analysis, and drafted the whole manuscript.

Paper IV

Iqbaal Abdurrokhman has designed the experiments, collected the experimental data, interpreted the results and drafted the manuscript.

Additional publications not included in the thesis:

Exploiting low-grade waste heat to produce electricity through supercapacitor containing carbon electrodes and ionic liquid electrolytes

Mazharul Haque, Iqbaal Abdurrokhman, Alexander Idström, Qi Li, Azega Rajaras, Anna Martinelli, Lars Evanäs, Per Lundgren and Peter Enoksson.

Submitted to Electrochimica Acta **(2021)**.

Contents

List of Figures

Chapter 1

Introduction

1.1 Background

One of the recurring challenges in human history has been the development of new functional materials that could meet the needs of the future. Those are the materials that can have a significant impact on how the world transforms. Imagine that, sometime in the future, a material has been developed with multiple functionalities; a material that is able to dissolve insoluble compounds, to work as a catalyst, to conduct ions and also to be reused. This material would be useful in a wide variety of industrial sectors or in energy conversion devices, examples being the textile and petroleum industries, for capturing dangerous gases, and in electrochemical devices like batteries, fuel cells or supercapacitor. This could sound like an utopia; however, since the discovery of room temperature molten salts in the 20th century, the idea of having multiple functions in one single compound, along with an ease of synthesis, is no longer a dream.

A molten salt is a liquid composed entirely of ions [1], and is a compound that can be used in electrochemical processes solving some limitations currently encountered while using aqueous media [2]. The combination of thermal stability, low vapor pressure and wide electrochemical window is the feature that makes molten salts appealing [3]. However, the use of molten salts is limited by their high melting temperature. For example, sodium chloride (NaCl) melts at the high temperature of 800 °C,

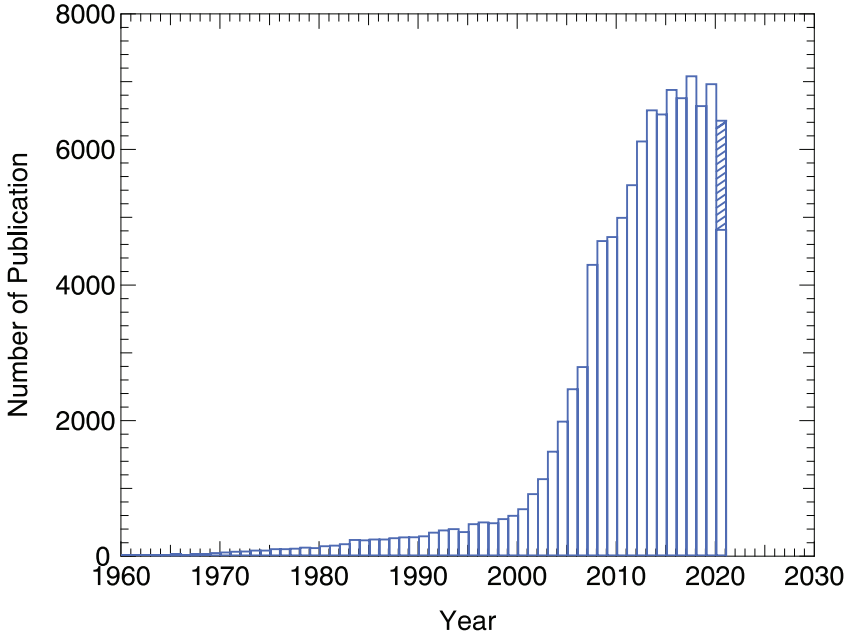

Figure 1.1: Number of published articles in the time period between 1960 and 2021, as found in the Scopus database and using the term "ionic liquids" as a keyword in the title field. The data for the year 2021 is only available for 8 months (updated to August 2021), wherefore the dashed bar represents the estimated number of articles extrapolating to the end of the year 2021.

while an example of intermediate temperature molten salt is the mixture of LiCl and KCl, with a melting point at 355 °C [3]. These high temperatures are not optimal for processes in the laboratory or industrial scale, since they are associated with a high energy consumption and can damage incompatible materials (degrading upon heating at high temperature). Therefore, the discovery of low temperature molten salts, able to form a liquid at room temperature, has been desired. Such low-melting salts have been discovered, and are currently referred to, in the industrial and scientific context, as ionic liquids. The synthesis, properties and possible applications of ionic liquids will be presented in chapter 2.

The research field pivoting around ionic liquids has expanded extremely rapidly, as reflected by the increasing number of publications during the years, Figure 1.1. Progresses in this field have led to the realization of various types of ionic liquids, for example room-temperature ionic liquids (RTILs), task-specific ionic liquids (TSILs), polyionic liquids (PILs), supported ionic liquid membranes (SILMs) and surface-active ionic liquids (SAILs) [4, 5].

To be precise, ionic liquids resemble the same properties as classic molten salts, with the distinction of having a considerable lower melting point. Ionic liquids also have a higher thermal stability, a wide electrochemical window, low volatility at ambient temperature and are able to conduct ions. The latter trait, in particular, has caused much interest in ionic liquids as electrolytes, for use in devices like batteries or proton exchange membrane fuel cells.

The proton exchange membrane fuel cell (PEMFC) is currently one of the most appealing technologies, because it can contribute to the challenge of decarbonisation related to the transport and stationary energy sectors. Recently, significant efforts have been devoted to improving the performance of proton exchange membranes, aiming at a higher ionic conductivity at higher operating temperatures, preferably at anhydrous conditions [6, 7]. In other words, new electrolytes able to conduct protons and providing a high thermal stability are required. In this context, ionic liquids, more specifically protic ionic liquids, have been highlighted as suitable candidates as proton conductors. In this thesis, I present my studies aimed to better understand some fundamental properties of protic ionic liquids, with focus on charge transport and interactions at the molecular scale. This knowledge is very important in the search for a material that can truly meet the requirements set for the next generation of PEMFCs, that is a material that can act as a proton conducting electrolyte and be stable at temperatures higher than 80 °C, ideally above 120 °C [7].

1.2 Objectives of this work

As mentioned above, protic ionic liquids are considered suitable candidates as proton carriers for use in intermediate temperature PEMFCs. Therefore, the objective of this thesis has been to investigate strategies that could possibly promote a high proton conductivity, such as mixing protic ionic liquids with a neutral compound or another protic ionic liquid, or making structural modification on the cation. Nevertheless, the scope of this thesis has been limited to the study of some imidazolium and triazolium-based protic ionic liquids.

More specifically, this thesis presents two main approaches. The first approach consisted in investigating the effect of adding a second compound on the phase behavior and the ionic conductivity of the pristine imidazolium based protic ionic liquid, which was done by either mixing the protic ionic liquid with a co-solvent or mixing with another protic ionic liquid with a similar cationic structure. The second approach consisted in studying the effect of structural modifictions on the cation on the physical and transport properties. In this spirit, alkyl chains of different lengths have been attached to an imidazolium cation and new cations derived from the base triazole have been realized.

1.3 Thesis outline

This thesis focuses on the synthesis and the characterization of protic ionic liquids as proton conducting materials with the aim to address some challenges related to the currently available fuel cell technology. Given the scientific context presented in **Chapter 1**, the organisation of this thesis is as follows. **Chapter 2** gives the background of ionic liquids such as history, synthesis, physicochemical properties and applications. **Chapter 3** presents the experimental methods used to characterize the protic ionic liquids considered in this study. **Chapter 4** summarizes the main findings related to the appended papers, covering the characterisation of protic ionic liquid mixtures (Paper I and Paper IV) and the modification of the ionic liquid's cation (Paper II and Paper III). **Chapter 5** concludes this thesis with some focus on possible future works.

Chapter 2

Ionic liquids

Ionic liquids, or low-temperature molten salts, are compounds that consist solely of ions. The development of ionic liquids with innovative properties for use in energy conversion devices has become an increasingly significant factor to solve one of the future challenges. By virtue of having a low vapor pressure, high ionic conductivity and tunable properties, they are reckoned as the next generation electrolyte in electrochemical energy devices, *e.g.* fuel cells and batteries. Yet, the properties of pure ionic liquids, or mixtures thereof, in relation to their use in electrochemical energy devices remain areas to investigate. The following chapter gives a glimpse of ionic liquids, including established synthesis procedures, their general properties, and the current applications at laboratory or industrial scales.

2.1 History and definition

Ionic liquids are defined as liquids composed solely of ions, *i.e.* cations and anions. In the so called "pre-ionic liquids era", they were referred to in the literature as room temperature molten salts, ionic fluids, liquid organic salts or organic low melting liquids. The history of ionic liquids can appear with some variations depending on the author that reports. Ethylammonium nitrate $[EtNH_3][NO_3]$, a compound that is now called an ionic liquid, was discovered and deliberately synthesised by Paul Walden back in the 19th century [3, 8, 9]. This is still today the pioneering work that most

scientists refer to, even though there is a record of an article dated 1880 presenting the synthesis of 1-methyl-3-ethylimidazolium iodide, also having properties that fall into the current definition of an ionic liquid [3]. $[EtNH_3][NO_3]$ is a protic ionic liquid obtained from the neutralisation reaction between amine and nitric acid [3]. Later on, this work became important as a reference for the determination of the ionicity in a number of ionic liquids, through the well known Walden's rule. In 1960s, an observation of a liquid salt was reported by Yoke *et al.* [10], who found that mixtures of copper(I) chloride and alkylammonium chlorides were liquid near room temperature. Additional ionic liquids having a low melting temperature were introduced in 1982 by Wilkes *et al.*, *i.e.* 1-alkyl-3-methylimidazolium chloride aluminium chloride ionic liquids ($[C_nC_1Im]Cl{-}AlCl_3$, where n=1–4) [9, 11].

In general, ionic liquids did not prompt significant interest until the revolutionary work of Wilkes and Zoworotko on the synthesis and characterization of water stable ionic liquids, published in 1992 [12]. This report defines the new beginning of the ionic liquids' field [9], and has inspired many researchers. They introduced ionic liquids derived from the imidazolium cation, namely 1-ethyl-3methyl-imidazolium tetrafluoroborate [EMIM][BF_4] and 1-ethyl-3methyl-imidazolium acetate [EMIM][AcO], which stay in a liquid state at ambient temperature. The synthesis was easy and could be done outside the environment of a glovebox. Moreover, these salts were stable towards hydrolysis at room temperature. This was revolutionary since the ionic liquids known to that time, like pyridinium and imidazolium chloroaluminates, were reactive to moisture, which could result in the formation of HCl, hence it was strictly required to treat them in a moisture-free environment or inside a glovebox [8, 12, 13].

2.2 Applications

Ionic liquids are known for having tuneable properties which allow them to be custom made for a wide variety of applications, such as in the oil and gas industry, as electrolytes in electrochemical energy devices, as lubricants, as solvents, and as catalysts [13], see Figure 2.1. During the current decade, we are witnessing the transition from

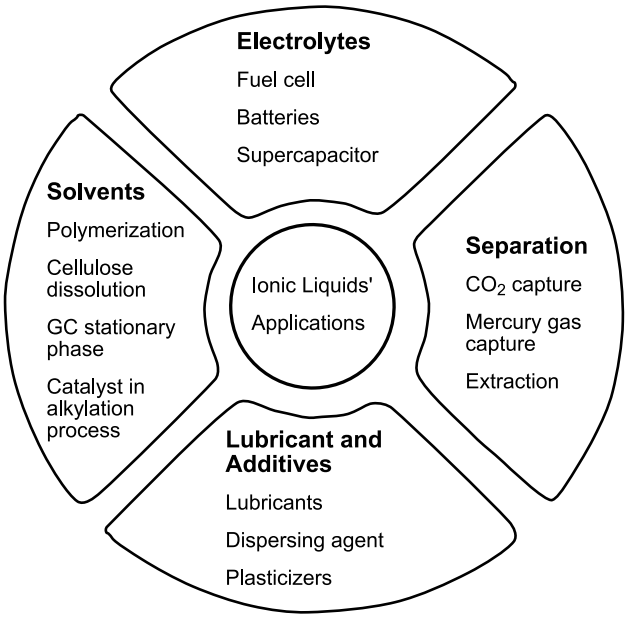

Figure 2.1: Overview of some possible applications of ionic liquids.

ionic liquids being solely a subject of laboratory scale research to ionic liquids also being interesting materials for industrial applications. For example, a big oil company like Chevron has replaced corrosive acids used in the alkylation unit with ionic liquids. Typically, the alkylation process requires hydrofluoric acid or sulfuric acid as the catalyst, in order to combine the low molecular alkane and alkene into a high-octane compound. The use of an ionic liquid instead, is advantageous because it is less corrosive, can act as a catalyst for the alkylation process, and is compatible with the already existing plant, which implies avoiding additional costs for replacing the processing equipment. This ionic liquid is known with the commercial name Isoalkyl^{TM} catalyst and has been licensed by Chevron and Honeywell [14]. Another example of an industrial scale application is the work done by Petronas Sdn Bhd and Queen's University Ionic Liquid Laboratories (QUILL) in the UK. This collaborative work focused on the use of a neoteric compound in a solid-supported ionic liquid phase (SILP) for capturing mercury gases. Mercury appears during the processing of natural gas in the oil and gas industry, is highly corrosive and can damage the equipment used. Moreover, it is known for its toxicity to human beings, hence a technology for capturing mercury to reach safety limits for mankind was really needed [15].

In the energy sector, the works of Armand *et al.* and Galiński *et al.* have inspired other scientists to conduct extensive research on ionic liquids for use as electrolytes in electrochemical energy conversion devices, *e.g.* batteries, fuel cells and supercapacitors [16–21]. The increasing demand for electric energy has greatly motivated this field of research. Nevertheless, the battery technology, *e.g.* the lithium battery, has faced safety issues related to flammability of the organic compounds used in the electrolytic phase. The commonly used electrolytes are flammable upon heating and reactive to air, and thus need to be replaced with non-flammable ion conducting compounds. In addition, the current problem of an increasing gas pollution comes mainly from the transport sector, resulting in the need of a technological shift from fossil fuels based to based on electrical energy. Here, the use of proton exchange membrane fuel cells (PEMFCs) can make a great impact, since a PEMFC can convert chemical energy into electricity without producing any polluting gas and is, theoretically, thermodynamically more efficient than a combustion engine, see Figure 2.2 for the basic principles of a PEMFC. In a PEMFC, a protic ionic liquid retained by a porous solid-like material, would act as the proton conducting material [7, 18, 22].

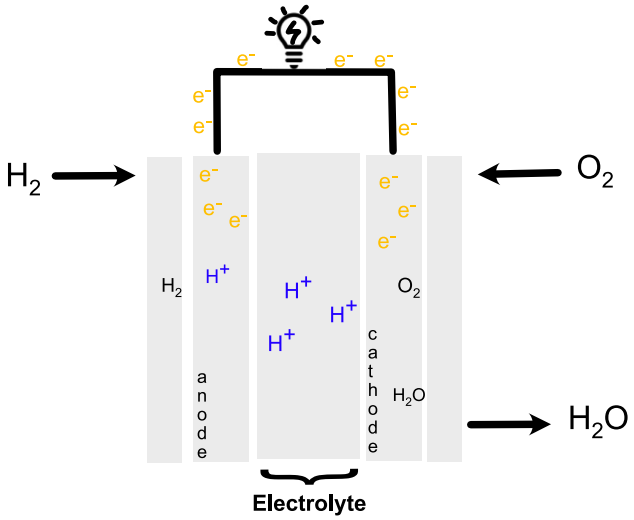

Figure 2.2: Schematic image of the working principles in a proton exchange membrane fuel cell (PEMFC). Currently known and available PEM materials limit the PEMFC to operate under humidified conditions and at temperatures below 80 °C.

2.3 Synthesis

The number of theoretically possible ionic liquids is approximately 10^6 (up to 10^{18} if ternary systems are included [13]) and the common methodology to synthesize them typically involves two steps. These include the synthesis of the desired cation followed by the formation of the anion by ion exchange, to obtain the desired ionic liquid, see Figure 2.3 [23]. Despite this theoretical simplicity, the synthesis of pure ionic liquids is in practice more difficult and limited by several factors, such as the miscibility with various solvents, the thermal stability and the tendency to absorb water from the surrounding environment.

The most common cations found in ionic liquids are derived from ammonium, phosphonium, sulfonium or five membered heterocyclic rings like imidazolium, pyrazolium, and triazolium, that due to their symmetry and large size contribute to lowering the melting point. In some cases, the synthesis of the cations by attaching other functional groups or longer alkyl chains require the alkylation reaction by mixing the respective cation with haloalkane in a basic environment. Common anions, on the other hand, are halides, nitrates $[NO_3]^-$, sulfates $[SO_4]^-$, tetrafluoroborate $[BF_4]^-$, hexafluorophosapte $[PF_6]^-$, triflate $[CF_3CO_2]$, and bistriflimide $[NTf_2]^-$. These anionic species are introduced by adding the corresponding acid to the cation of choice. Among

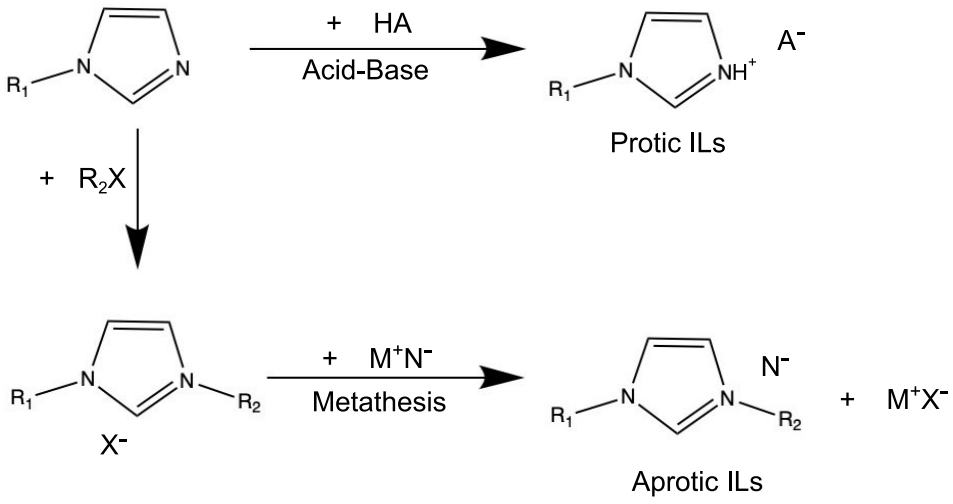

Figure 2.3: Schematic of the synthesis paths used to obtain ionic liquids, showing the cases of a protic (top) and an aprotic (bottom) imidazolium cation.

all possible anions, fluorinated ones are commonly selected since they result in lower viscosities as a consequence of weaker van der Waals interactions [24, 25]. In the case of aprotic ioic liquids, the anion is derived from a metathesis reaction or ion exchange. Protic ionic liquids, on the other hand, are obtained by a simple synthesis route through a Brønsted acid-base neutralization reaction. Cation-anion pairs can be judiciously chosen to tune the physicochemical properties of ionic liquids, such as melting point, viscosity and liquidous range; typically, cations with a low symmetry contribute to a lower melting point while anions often come from inorganic or organic base.

The long established protic ionic liquid, ethylammonium nitrate or $[EtNH_3][NO_3]$, is obtained by the neutralisation reaction between ethyl-amine and nitric acid [8]. The main focus of this thesis is on protic ionic liquids, which can be synthesized in the same manner, by simply mixing a Brønsted acid and a Brønsted base at equimolar ratios. Angell and Yoshizawa have thoroughly investigated the degree of proton transfer from a Brønsted acid to a Brønsted base, finding that this is a function of ΔpKa, *i.e.* the stronger the acid or the base the greater the driving force for the reaction to occur. They also proposed that a ΔpKa larger than 10 is required to achieve a full proton transfer [24, 26].

2.4 Properties

An overview of the ionic liquids' properties and the factors that govern them is presented in this section. The size of both cations and anions, the nature of molecular interactions, and the strength of interactions will all affect not only the thermal stability but also the transport properties, such as viscosity, ionic conductivity, and self-diffusivity of the ionic species. Understanding how physical and transport properties correlate is key to develop proton conducting ionic liquids for use in proton exchange membrane fuel cells.

2.4.1 Thermal stability

The thermal stability of ionic liquids is a critical property for use in high-temperature processes, *e.g.* as solvents in a high temperature reaction, thermal energy storage (TES) and heat-transfer fluids (HTFs), high-temperature lubricants, and high recovery in manufacture [27]. Moreover, next-generation PEMFCs operating at higher temperatures could be developed by use of thermally stable ionic liquids. However, not all ionic liquids are very stable at high temperatures, and some easily decompose and/or evaporate. This can generate impurities and cause environmental problems, as volatile organic compounds already do. Thermogravimetric analysis (TGA) is the most com-

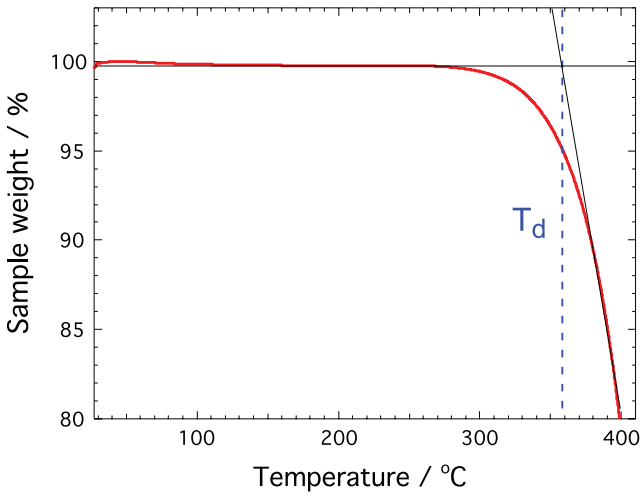

Figure 2.4: Typical TGA curve obtained from a thermogravimetric experiment, showing the case of the ionic liquid $[C_2HIm][TFSI]$. A simple method used to determine the decomposition temperature, T_d, is also shown.

mon method to determine the thermal stability of ionic liquids, usually by a single linear heating scan over a wide temperature interval. The thermal stability of ionic liquids is usually determined by a characteristic mass loss at a high temperature, *i.e.* the decomposition temperature, T_d, or the onset temperature, T_{onset}, see Figure 2.4.

Mass losses in ionic liquids are caused by two phenomena; decomposition and evaporation. Decomposition refers to the degradation of molecular species induced by a chemical reaction, while evaporation is a physical process from the liquid to the gaseous state without the formation of new compounds. The molecular structure of cations and anions plays an important role in the thermal stability of the ionic liquid. For example, while keeping the total number of carbon atoms in the attached alkyl chain(s) constant, the volatility is lower for an ionic liquid with an asymmetric cation than for an ionic liquid whose cation has a symmetric structure [28].

2.4.2 Molecular interactions

Molecular interactions in ionic liquids are complex and depend on the charge as well as on the molecular and electronic structure of the constituting ions. Thus, understanding molecular interactions is challenging, yet crucial to design task specific ionic liquids. Coloumbic interactions, hydrogen bonding, and dispersion forces are the interactions at simultaneous play. In principle, these interactions can be studied by a number of experimental techniques, primarily by vibrational (Raman and infrared) and NMR spectroscopy [29–32].

The main feature that distinguishes protic from aprotic ionic liquids is the proton transferred from the acid to the base, which results in the formation of proton donor and proton acceptor sites and thus in the build up a hydrogen-bonded network. Hydrogen bonds can also form in aprotic ionic liquids, but they are typically weaker and involve the hydrogen atoms in the alkyl groups or, more likely, the hydrogens in the aromatic ring of the cation as well as the electronegative atoms on the anion, such as O^-, F^-, and N^-. In protic ionic liquids, the hydrogen bond is stronger and typically involves the protonated -NH site on the cation [33]. Protic cations have a H-atom covalently bonded to a charge carrying nitrogen or phosphor atom, and based on the

general measure with respect to 'donor strength', the order of hydrogen bond strength is known to be O–H > N–H > S–H > C–H. To summarize, protic ionic liquids form stronger and more directional hydrogen bonds than their aprotic counterparts [31]. Established experimental and computational methods can be used to demonstrate the existence, and nature, of hydrogen bond interactions in ionic liquids [34–37].

2.4.3 Nanostructure

Bulk ionic liquids were initially thought of as common solvents, *i.e.* as homogeneous molecular systems. However, recent experiments and computational results indicate that ionic liquids can form heterogeneous structures at the nanoscale [38]. The degree of nanostructuration in ionic liquids depends on several aspects; coloumbic interaction, packing geometry, cation-anion structure and hydrogen bonding [38]. For example, the nanostructure in ionic liquids becomes more evident as the alkyl chain on the cation or the anion increases; this is because the segregation of charged and uncharged species becomes more pronounced. Different anion types also influence the ionic liquids' nanostructure, as recently shown by comparing trihexyl (tetradecyl)phosponium chloride $[P_{6,6,6,14}][Cl]$ with trihexyl (tetradecyl)phosponium bistriflimide $[P_{6,6,6,14}][NTf_2]$, the $[Cl]^-$ anion leading to more defined nanostructures than the $[NTf_2]^-$ anion [39].

A variety of experimental techniques can be employed to describe the bulk ionic liquid's structure with segregated polar and non-polar domains, *e.g.* small angle neutron scattering (SANS) and small angle X-ray scattering (SAXS) [39]. Russina and co-workers have investigated and explained the structural heterogeneity in 1-alkyl-3-methylimidazolium bis(trifluoromethane)sulfonylamide ($[C_nmim][NTf_2]$), n varying from 1 to 10, by the use of small-wide angle X-ray scattering (SWAXS). Bragg's law $d = 2\pi/q_{max}$, where d is the correlation length and q_{max} is the peak position at maximum intensity, was used to describe three distinct diffraction peaks. The strongest intensity peak in the low q region, 0–0.5 $Å^{-1}$, is highly dependent on the length of the alkyl chain, and is a signature of the nanostructural heterogeneity observed despite the liquid state [40].

2.4.4 Transport properties

2.4.4.1 Fluidity

The high conductivity of liquid electrolytes is generally associated to a low viscosity. Viscosity describes the internal resistance of a fluid to flow, and has the units of poise or Pa·s. The viscosity in ionic liquids depends on intrinsic factors, *e.g.* the ions' size, ion-ion interactions (coulombic interaction, van der Waals force and hydrogen bonds), and extrinsic factors like temperature and pressure. For example, delocalisation of the charge on the anion, such as through fluorination, decreases the viscosity by weakening hydrogen bonding. Consequently, fluorinated anions are preferably used in ionic liquids. Another aspect that affects the viscosity in ionic liquids is the structure of the cation. A thorough investigation of a series of 25 ionic liquids by Greaves *et al.* showed that increasing the length of the alkyl chain attached to the cation increases the viscosity because of the stronger Van der Waals interactions. Interestingly, that study also revealed that the substitution of functional group by alkyl chains has a significant effect on the viscosity and is attributed to stronger hydrogen bonding, ion-ion interactions and asymmetry of the molecules [41].

2.4.4.2 Self-diffusion

Diffusion, a phenomenon of particles in motion, depends on several factors such as pressure, temperature, and concentration. For a system in which diffusion occurs in the x-direction as a consequence of a concentration gradient, it can be written as follows:

$$\bar{J} = -D\frac{dC}{dx} \tag{2.1}$$

where J is the molecular flux, D is the self-diffusion coefficient, and C is the concentration. D represents the rate of motion in a certain area over a unit time and has the units m^2/s. In classical hydrodynamic, the Stokes-Einstein equation relates D of a particle (or a molecular species) to its effective hydrodynamic radius r_s, the viscosity of the medium η, the temperature T, the shape factor c (4 to 6), and the Boltzman constant k_B (eq. 2.2)

$$D = \frac{k_B T}{c\pi\eta r_s} \tag{2.2}$$

Compared to the gaseous state, in liquids molecules are more densely packed and display smaller self-diffusion coefficients. In thermodynamic equilibrium conditions, the individual molecules in a liquid move by a random translational motion, also called Brownian motion. In this work, diffusion NMR is employed to study the self-diffusion of the ionic species in protic ionic liquids, with some emphasis on the proton's dynamics. The occurrence of a Grotthuss, or hopping, mechanism can be indicated by protons diffusing faster than their parent molecules.

2.4.4.3 Ionic conductivity

In general, ionic conductivity relies on a variety of aspects; the concentration of charge carriers (C), the charge they carry (Z) and their mobility (μ). According to this definition, the ionic conductivity, σ, can be expressed as:

$$\sigma = (|Z|F)C\mu \tag{2.3}$$

The absolute symbol is to ensures that the conductivity value is always a positive number, F is the Faraday's constant, and σ is measured in Siemens·cm^{-1}.

The idea of using ionic liquids as new electrolytes in next generation PEMFCs originates from their high ionic density coupled with a relatively low viscosity. In reality, however, the ionic conductivity can be affected by the presence of ion-pairs and/or neutral species, reducing the actual concentration of ionic species. Experimental results presented by Yaghini *et al.* [30] show that the conductivity of aprotic ionic liquids is higher than that of their protic analogous, due to higher inter-ionic interactions and hence a higher viscosity in the case of protic cations.

2.4.4.4 Proton transport mechanisms

There are two main types of proton transport mechanisms; the vehicular and the Grotthuss (or proton hopping) mechanism, as illustrated in Figure 2.5. In the vehicular mechanism, the proton is transported by the host molecule through a purely translational movement, whereby the protonic migration is limited by molecular diffusion. In the Grotthuss mechanism, the proton motion is decoupled from the host molecule

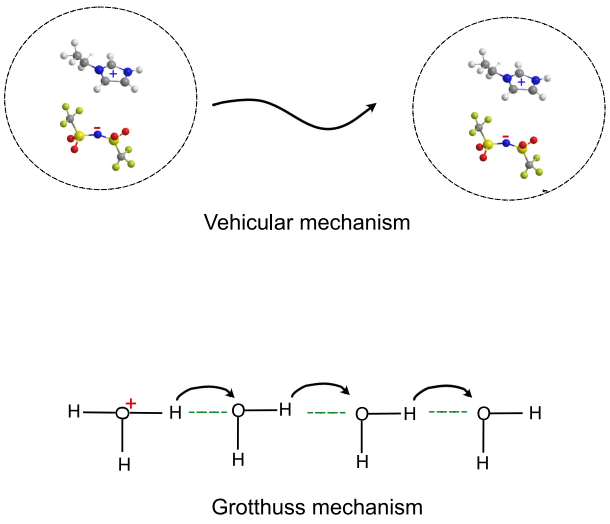

Figure 2.5: The vehicular (top) and the Grotthuss (bottom) mechanisms of proton transfer illustrated for the cases of an ionic liquid and water, respectively.

and moves through structural diffusion *via* hydrogen bonds [42]. The formation and breaking of hydrogen bonds is an essential prerequisite for this process to occur. The Grotthus mechanism requires a small activation energy Ea $<$ 0.4 eV, while the vehicular mechanism requires a larger energy contribution, Ea $>$ 0.4 eV [43].

In protic ionic liquids, the proton can be transported by the vehicular or the Grotthuss mechanism, or by a combination of these two. Appropriate analytical methods are necessary to distinguish between these cases. NMR spectroscopy can be employed to study transport properties, more precisely pulsed-field gradient (PFG)-NMR has been used to measure, when possible, the self-diffusion of ionic and protonic species. One way of examining the occurrence of the Grotthuss mechanism is through the D_H/D_{cation} ratio, which is significantly above unity in the case of a decoupled proton motion [30, 44]. To conclude, the dynamics of the exchangeable proton in protic ionic liquids is crucial to investigate and may be promoted by either adding a second compound able to act as a proton acceptor through hydrogen bonds or by modifying the cation's structure such that the acidity of the protonic site is increased.

Chapter 3

Experimental methods and procedures

This chapter gives a brief description of the procedures used in each of the characterisation techniques included in this work. For PEMFC applications, there are some requirements such as higher thermochemical stability and, if possible, a wide temperature range of the liquid state in order to fully utilize the potential of protic ionic liquids. Thus, appropriate thermal analyses are required, such as thermogravimetric analysis and differential scanning calorimetry. Also, the physicochemical properties of the ionic liquids are determined by the interaction at molecular level, which can be studied by vibrational spectroscopy. Additionally, transport properties (*e.g.*, ionic mobility) are crucial to investigate, because related to the application as proton conductors, therefore impedance spectroscopy as well as diffusion NMR have been employed.

3.1 Thermal characterization

Solid or liquid materials can change their properties when exposed to heat, for example during heating or cooling treatments. Thermal methods of characterization are generally simple, yet they can provide a wealth of useful information to materials scientists. One possible application of the protic ionic liquids treated in this thesis is as electrolytes in intermediate temperature (above 120 °C) PEMFCs; therefore, it has been critical to investigate their thermal stability by thermal analyses, more precisely by means of thermogravimetric analysis (TGA) and differential scanning calorimetry

(DSC). This section aims to explain the working principles behind TGA and DSC, but it also describes the experimental procedures used in my work.

3.1.1 Thermogravimetric analysis (TGA)

Thermogravimetric analysis (TGA) is widely used to study the thermal stability of materials by analysing the mass changes occurring as a function of temperature or time, in a controlled gas atmosphere. The mass loss recorded during a TGA experiment can give information about decomposition kinetics, lifetime and thermal stability, as well as about oxidative stability. The material can loose or gain mass during the heating processes due to several phenomena:

1. Evaporation of volatile compound
2. Oxidation of organic material in contact with air or pure oxygen
3. Thermal decomposition

A number of factors should be considered when performing TGA experiments, such as sample preparation, heating rate (there are two options here; heating by a constant heating rate, also referred to as dynamic mode, or heating at a constant temperature, also referred to as isothermal mode), type of crucibles and nature of the purging gas. Various purging gases can be used for studying the degradation or decomposition behaviour of materials [45]. In this work, in order to resolve two adjacent events occurring at proximate temperatures, we have also plotted the first derivative of the mass change curve with respect to temperature (Paper III). One representative plot obtained from a TGA experiment including a derivative thermogravimetric (DTG) curve is shown in Figure 3.1, for the representative case of 1-ethyl-1,2,4-triazolium triflate, [C_2HTr_{124}][TfO].

In this work, the analysis of protic ionic liquids was carried out using a TGA/DSC 3+ from Mettler Toledo, equipped with an autosampler and able to cover the temperature range from 25 °C up to 1200 °C. In this thesis, the samples (typically 3-20 mg) were placed in 100 μl aluminum crucibles, and the temperature was typically set to

scan from 25 °C to 400 °C (Paper I and II) and from 25 °C to 500 °C (Paper III and IV). The crucibles were kept under nitrogen flow (Paper I, III IV) or under air flow (Paper II).

3.1.2 Differential scanning calorimetry (DSC)

In ionic liquids, the temperatures of crystallization (T_c), melting (T_m) and glass transition (T_g) are crucial to be identified, since they affect or even limit their application, but also define the storage conditions. Thus, the use of DSC is valuable to material scientists who work with this type of ionic materials. A DSC experiment is easy to perform, requires little sample preparation, and provides a wealth of useful information. In practice, DSC is sensitive to the heat flow difference between a sample and a reference as a function of time and temperature, a difference that is monitored during heating or cooling scans. Qualitative and quantitative results on physical or chemical properties can be detected by analyzing [46]:

1. Melting and enthalpy of fusion
2. Crystallisation and supercooling
3. Solid-solid and solid-liquid transitions

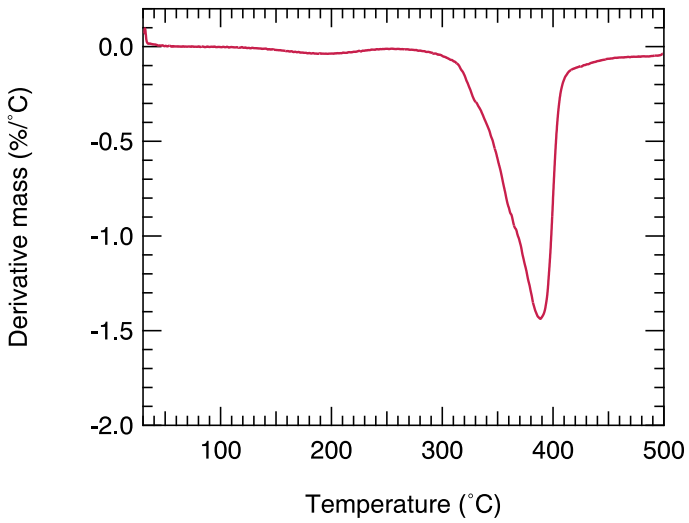

Figure 3.1: Example of a first derivative thermogravimetry (DTG) curve, recorded for the protic ionic liquid 1-ethyl-1,2,4-triazolium triflate [C_2HTr_{124}][TfO].

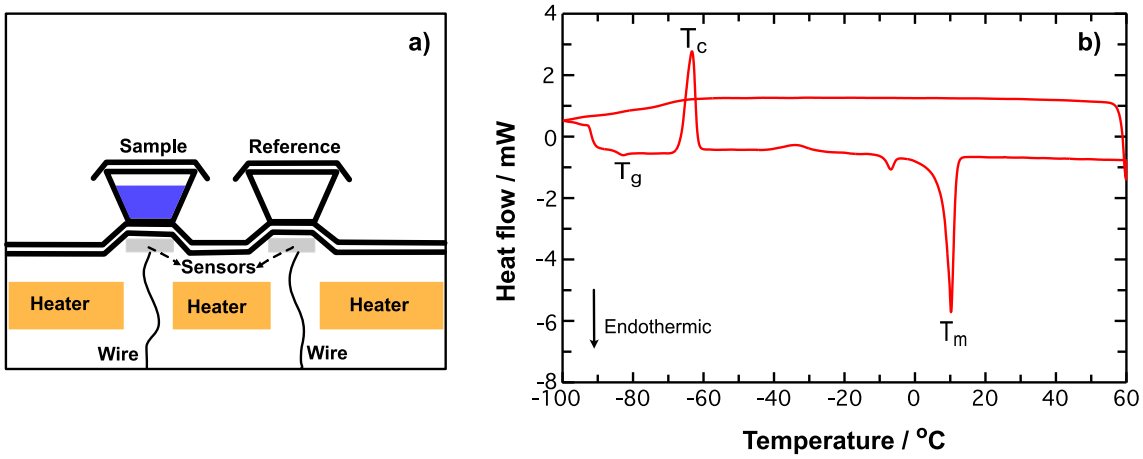

Figure 3.2: Schematic diagram of the DSC chamber used in this thesis (a) and a typical heat flow curve obtained during a DSC experiment for the representative case of 1-ethyl-imidazolium bistriflimide [C_2HIm][TFSI] (b).

Inside a DSC chamber there are two platforms for the sample and the reference crucible (typically an empty one). The crucibles are placed over the DSC sensors which are connected through a thin ceramic disc to the metallic part of the furnace, see Figure 3.2a. As the temperature of the furnace is increased, heat flows to the discs and the crucibles. In principle, DSC measures the heat flow in or out of a sample. The heat flow is either exothermic or endothermic, and its direction is conventionally indicated in a DSC plot (see Figure 3.2b). The heat flow is exothermic upon release from the sample, for example in the event of crystallization, while it is endothermic when it is absorbed by the sample, for instance during phase transition from solid to liquid. By a DSC experiment, it is also possible to measure the heat capacity change, *i.e.* the glass transition temperature, T_g, typically seen as a step change in the baseline of the DSc curve. T_g is the temperature at which a glass forming material transition from the liquid state to a rigid and disordered state (during cooling) [46, 47]. A typical DSC plot recorded for an ionic liquid is shown in Figure 3.2b.

All the calorimetric measurements were performed with a DSC2 instrument from Mettler Toledo equipped with a Huber TC-125MT Intracooler cooling system. This system can work from -100 to 500 °C, at heating rates variable from 2 to 300 K·min^{-1} and cooling rates as high as 50 °C·min^{-1}. The samples were always placed in 40 μl alu-

minum crucibles and the sample mass was typically kept between 3 and 7 mg. Nitrogen was used as the purging gas during the DSC experiments. In Paper I, the temperature spanned from -120 to 130 °C, and the protic ionic liquid-ethylene glycol mixtures were first quickly cooled from 25 °C to -120 °C at a cooling rate of 20 °C·min^{-1}, followed by a subsequent heating scan at a rate of 10 °C·min^{-1} up to 130 °C. In Paper II, the cooling and heating rates were set to 10 and 5 °C·min^{-1}, and the covered temperature window spanned from -100 to 60 °C. In Paper III, the DSC experiment was performed by using two different strategies; in order to promote crystallization, a slow cooling rate of 2 °C·min^{-1} was chosen, while to promote the formation of the glassy state a faster cooling rate of 10 °C·min^{-1} was selected. In Paper IV, the cooling was performed at 20 °C, followed by a subsequent heating at 5 °C. In both Papers III and IV, the DSC experiments covered the temperature range from -100 °C to 60 °C.

3.2 Vibrational spectroscopy

Vibrational spectroscopy has been used to investigate the local interactions in the protic ionic liquids. In my work, I have used both Raman and infrared spectroscopies that, although being principally different in their experimental design, are complementary techniques. Raman is more sensitive to symmetric vibrations of non polar molecules, while asymmetric vibrations of polar molecules are better seen by infrared. Vibrational spectroscopy can be used for a wide variety of samples and can provide information both qualitatively and quantitatively. Vibrational spectroscopy offers several advantages, such as ease of sample preparation, being a non invasive method, and only small amounts of sample are needed. In the context of my thesis, vibrational spectroscopy has been used to study the nature of cation and anion interactions, molecular conformation and the nature of hydrogen bonding in pure or mixed protic ionic liquids [48–50].

The basic principle of vibrational spectroscopy can be described by the classical harmonic oscillation theory of two bonded atoms, considered as two vibrating masses (m_1 and m_2) connected by a spring representing the chemical bond, according to equa-

tion 3.1:

$$\bar{v} = \frac{1}{2\pi c}\sqrt{\frac{k}{\mu}} \tag{3.1}$$

where $\bar{v}$ is the vibrational frequency in inverse centimeters (cm^{-1}), k is the force constant of the bond, c is the velocity of light and μ is the reduced mass of the system, *i.e.*

$$\mu = \frac{m_1 m_2}{m_1 + m_2} \tag{3.2}$$

As shown in equation 3.1, a higher force constant (or a stronger bond) results in a higher vibrational frequency. Heavier atoms (*i.e.* a higher value of μ) result in lower frequencies of vibration.

3.2.1 Raman spectroscopy

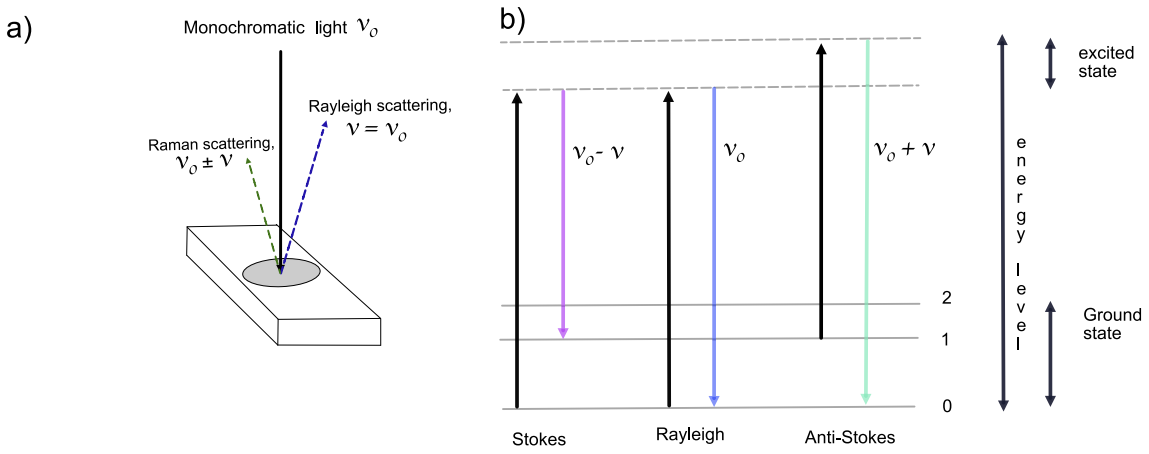

Figure 3.3: Basic principles in Raman scattering, showing the incident and scattered light (a) and the energy levels involved in the Rayleigh, Stokes and anti-Stokes type of scattering (b).

In Raman spectroscopy, the measurement is based on a scattering process during which light and matter interact. The incident light is intense and monochromatic, and is scattered by the material elastically or inelastically. Lasers are the typical source of incident light, and can deliver beams with a focal volume at the sample of about 1 - 2 micrometers in diameter, depending on the objective as well as the wavelength of the laser in use. In Rayleigh scattering, light is scattered elastically with no change in energy, hence in frequency, and v = v_0. In Raman scattering, the energy of the

scattered light is affected by the interaction with matter and the frequency is v_0 + v in the case of anti-Stokes and v_0 - v in the case of Stokes scattering, as illustrated in Figure 3.3 [48, 50]. Rayleigh scattering is millions of times more frequent than Raman scattering, and needs to be blocked from reaching the detector for a proper record of Raman spectra.

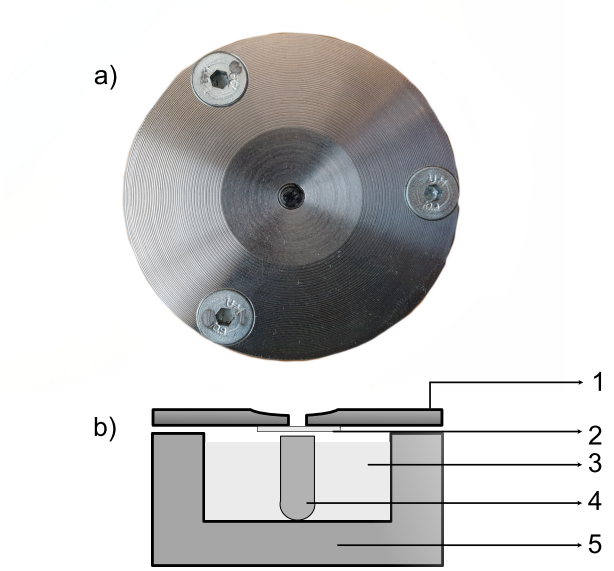

Figure 3.4: Custom made gas-tight Raman cell, with the top view and its cross sectional view illustrated in a) and b) respectively. The different parts of the cell are as follow: (1) Stainless steel lid, (2) Round glass cover, (3) Glass tube holder (a foam), (4) Glass tube, and (5) Stainless steel body.

In this work, Raman spectra were recorded with a InVia Reflex Raman spectrometer from Renishaw® equipped with four lasers emitting light with a wavelength, λ, of 514, 532, 633, and 785 nm. The laser emitting light with λ = 785 nm was used for collecting the Raman spectra of all the protic ionic liquids included in this thesis. The spectrometer used is also equipped with three different gratings, with 1200, 1800 and 2400 l/mm. In Paper I and Paper II, the measurements were performed using the 785 nm laser together with a 1200 l/mm grating, the laser power was set to 3 mW (at the source), and the spectrometer was calibrated with a Si wafer to the vibrational mode at 520.6 cm^{-1}, while the spectral resolution was 2 cm^{-1}. The samples were poured into NMR tubes and measured at room temperature. Typically, spectra were collected covering the spectral range 80 – 4000 cm^{-1} and 10 to 20 accumulations were collected,

each with 10 s of exposure time.

In Papers III and IV, the Raman experiments were performed using a custom made, gas tight, Raman cell made of stainless steel, see sketch in Figure 3.4. The liquid sample was placed in the glass tube inside the Raman cell and prepared in the glovebox. Again, the 785 nm laser was used, at a nominal power of 10 % and using a diffraction grating with 1200 l/mm. The spectra were collected covering the spectral range 100 – 4000 cm^{-1} accumulating 8 scans (Paper III) and 5 scans (Paper IV) with 10 seconds of exposure time.

3.2.2 Infrared spectroscopy

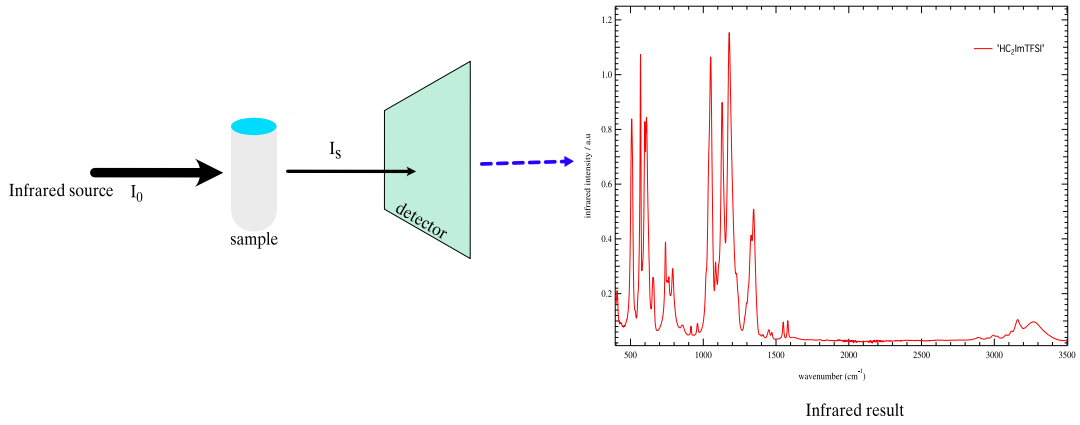

Figure 3.5: Principles of infrared spectroscopy and a typical infrared spectrum recorded for $[C_2HIm][TFSI]$.

Infrared spectroscopy is widely utilized in research programs performed in both academia and industries. It can provide crucial information about the chemical properties of a material, requiring a very small sample amount and in short period of experimental time. The sample is irradiated with an infrared source with intensity I_0 that, by interacting with the molecules in the material investigated, is absorbed, transmitted or reflected. Some of the infrared radiation is transmitted by the sample, I_s, and collected

by a detector, then plotted in intensity versus frequency plots, see Figure 3.5. In the case of infrared spectrometers used in reflection mode, one could further select specular reflectance, diffuse reflectance, or attenuated total reflectance (ATR). The latter has been used in this thesis work. Molecular vibrations are associated to changes in bond lengths and bond angles, and can be classified as wagging, stretching, scissoring, rocking, bending and twisting.

The infrared spectra of neat or mixed protic ionic liquids were collected using a Perkin Elmer spectrometer, equipped with an ATR crystal and suitable for investigating liquid and gel-like samples. Droplets of the liquid were poured over a single reflection diamond crystal, covering the spectral range 400 – 4000 cm^{-1} by accumulating 20 scans in Paper I, 32 scans in Paper II, 8 scans in Paper III and 16 scans in Paper IV. The spectral resolution was 2 cm^{-1}. The measurements reported in Papers I and II were performed in open air, while those discussed in in Papers III and IV were preformed under nitrogen gas flow; in all cases infrared spectra were collected at room temperature.

3.3 Nuclear magnetic resonance (NMR)

Nuclear magnetic resonance (NMR) spectroscopy is an established, versatile method to qualitatively analyse the structure of organic molecules, but it is also used for quantitative purposes, *e.g.* for purity assessment. NMR spectroscopy is based on the spin behavior of atomic nuclei, and common nuclei that possess a spin are ^{1}H, ^{15}N, ^{13}C, and ^{19}F. The nuclei of interest in the studies included in this thesis are mainly the proton and the fluorine. A nucleus is a charged particle, that generates a magnetic field when it spins. When an external magnetic field (B_0) is applied, the magnetic orientation of the nucleus can orient aligned or against the applied field, as shown in Figure 3.6. In NMR, the spectrum intensity is plotted as a function of chemical shift. The chemical shift is commonly given in ppm, and different nuclei in a molecule give rise to different chemical shifts.

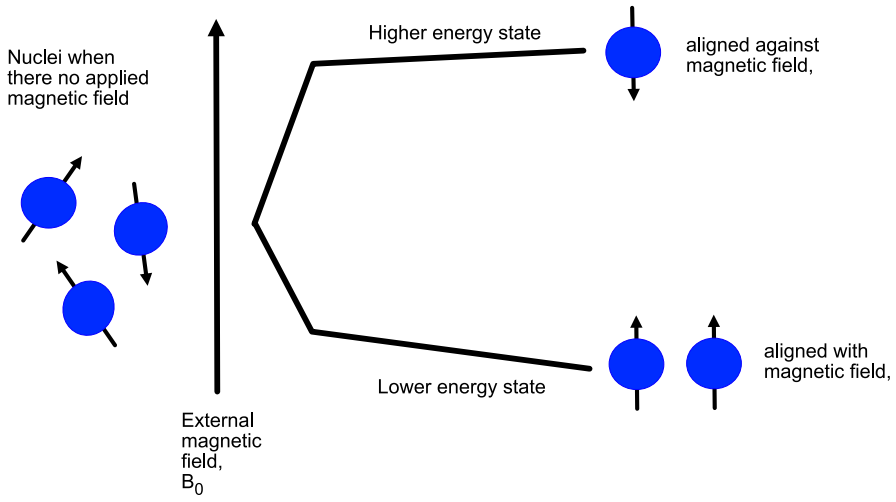

Figure 3.6: Spin states of proton in the presence of external magnetic field (B_0).

In this thesis, qualitative NMR experiments were performed using a Varian 400-MR spectrometer equipped with a OneNMR probe. The compound in Paper III was dissolved in DMSO-d_6 and loaded in common 5 mm NMR tubes. The spectra were collected at 25 °C, using standard pulse sequences and acquisition settings for qualitative hydrogen and carbon spectral analysis. The relaxation time during the acquisition of the hydrogen spectrum was set to 120 s to fully relax the hydrogen. The NMR spectra of protic ionic liquids were collected using a Bruker Avance III 700 MHz spectrometer equipped with a 5 mm QCI cryoprobe ($^{1}H/^{19}F/^{13}C/^{15}N$). The ionic liquids were placed inside coaxial NMR tubes filled with DMSO-d_6. The spectral analysis was done using the MestReNova 10.0.0 software.

$$Px = (A_x/A_s)(N_s/N_x)(W_s/W_x)(M_x/M_s)P_s \tag{3.3}$$

Equation 3.3 was used for quantitative NMR (qNMR) in Paper III, where A is the area under the peak, N is the number of nuclei (proton or fluorine), W is the substance amount taken for the measurement, and M is the molar mass. The subscript *x* refers to the analyte and *s* to the internal standard. Triplicate samples were prepared in the moisture-free atmosphere of a glove box in order to avoid interference from absorbed water. The analyte and internal standard (4-Fluoroacetophenone) were mixed at equal amounts of mass, followed by adding 600 μl DMSO-d_6 in to a 5 mm NMR tube. The

samples were analysed using either a Bruker Avance III 700 MHZ equipped with a 5 QCI cryoprobe (^{1}H/^{19}F/^{13}C/^{15}N) or a varian VNMR-S 500 MHz equipped with a 5 mm pulse field gradient dual broadband probe (^{1}H-^{19}F/^{15}N-^{31}P). All the spectra were obtained at room temperature; *i.e.* at 25 °C. The purity calculation was based on the purity calculator script in MestReNova software and using equation 3.3 [51].

3.4 X-ray scattering

In X-ray scattering, the pattern resulting from scattered X-rays, caused by differences in the average electron density, is analysed. X-ray scattering can be used to study the structure, shape, size and structural orientation in a material. This method enables to analyse any object displaying a spatial variation in electronic density (contrast), and the sampled material could be in the liquid or solid state, amorphous or crystalline, but the information on voids may also be captured (*e.g.*, pores, blisters, cracks, crazes) [52, 53]. Figure 3.7 illustrates the basic principles of an X-ray scattering event.

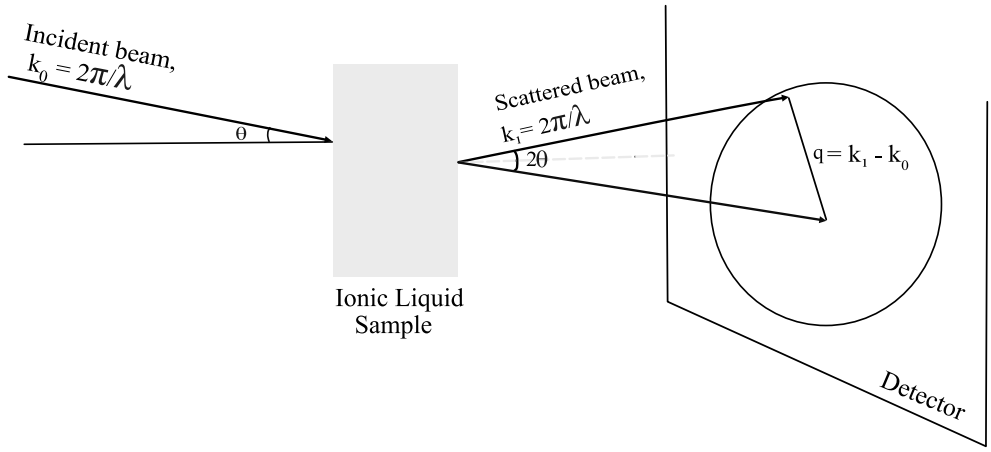

Figure 3.7: Schematic illustration of the working principles in X-ray scattering [53].

In the case of elastic scattering, the incident and scattered X-ray wave have equal energy, and $|k_0| = |k_1| = 2\pi/\lambda$. However, the scattered rays have a different direction and the scattering angle is described by 2θ. The wave vector, q, defines the position of

the collected X-ray on the detector.

$$q = k_1 - k_0 \tag{3.4}$$

$$q = |q| = \frac{4\pi}{\lambda} sin\theta \tag{3.5}$$

The dimension of the scattering object, d, can be calculated from the position of the diffraction peak q, based on Bragg's law:

$$d = \frac{2\pi}{q} \tag{3.6}$$

In this study, a Mat:Nordic SAXS/WAXS/GISAXS instrument, available at the Chalmers Material Analysis Laboratory (CMAL), was used to collect the data presented in Paper II. This instrument can be set to measure in three q regions: 0.07 – 2.7 $Å^{-1}$ (wide angle X-ray scattering, WAXS), 0.02 – 0.7 $Å^{-1}$ (medium angle X-ray scattering, MAXS), and 0.007 – 0.25 $Å^{-1}$ (small angle X-ray scattering, SAXS). In order to obtain correct and reliable data, a standard calibration is needed, and silver behenate (AgBeh) was chosen as the reference to accurately calibrate the investigated q range. Since in ionic liquids a nanostructuration may form, the interesting structural features were captured by setting the X-ray spectrometer to operate in the WAXS mode, *i.e.*, by accessing the q range 0.07 – 2.2 $Å^{-1}$. All measurements were performed at ambient temperature.

3.5 Transport properties

3.5.1 Fluidity

Newton described that the resistance to motion of a fluid is attributed to an "internal friction", which we call viscosity. He postulated that the force (F) per surface area (A) required to maintain the motion of a fluid between two plates is proportional to the velocity gradient (u/h) and to viscosity (η), as expressed in equation 3.7. For simplicity, this is often illustrated as a fluid sandwiched between two parallel plates, as shown in Figure 3.8 [54, 55].

$$\frac{F}{A} = \eta(\frac{u}{h}) \tag{3.7}$$

$$\tau_{xy} = \eta\dot{\gamma}_{xy} \tag{3.8}$$

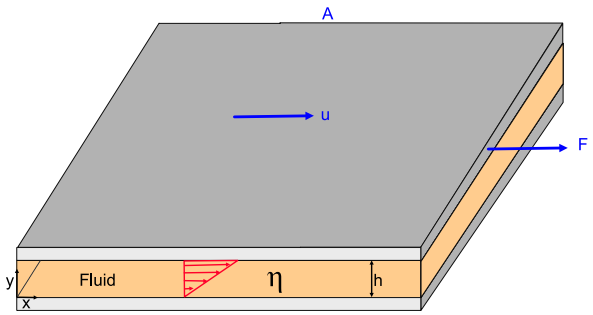

Figure 3.8: Simple representation of a viscous fluid (orange) placed between two parallel plates (grey). The bottom plate is fixed and the upper plate is moved with the velocity u.

Equation 3.7 can be rewritten in terms of shear stress and shear rate, as shown in equation 3.8, where τ_{xy} is the shear stress in the *x* direction and $\dot{\gamma}_{xy}$ is the shear rate deformation of the fluid. By convention, a liquid that follows Newton's postulate is called a Newtonian liquid, and its shear rate is proportional to the shear stress; otherwise, it is called a non-Newtonian liquid. There are various ways to measure viscosity, such as the capillary method, the falling sphere method, the plastometer method, and the rotational rheometry method (parallel or cone and plate) [56].

The viscosity of the ionic liquids studied in both Papers I and II was determined using cone and plate rotational rheometry. In Paper I, the viscosity was measured by an Antoon Paar MCR 300 instrument with cone and plate geometry with a diameter of 50 mm, an angle of 1°, and a trunctuation gap of 52 μm. Whilst in Paper II, the DRH 3 from TA instrument equipped with a peltier plate was used, which has the ability to measure in a wide temperature range from -40 to 200 °C with an accuracy of $\pm$ 0.1 °C; the cone and plate geometry with an angle of 1°, a trunctuation gap 26 μm, and 40 mm of diameter, was used. All measurements were performed at room temperature.

3.5.2 Ionic conductivity

A broadband dielectric spectrometer (BDS) was used to study the ionic conductivity of protic ionic liquids. By dielectric spectroscopy, which is directly related to impedance spectroscopy, ionic conductivity values could be estimated. These were extracted from the plateau region of the frequency dependent conductivity (*i.e.*, the real part of conductivity, σ'). The cell set up used for the dielectric measurement performed in this thesis is shown in Figure 3.9. The sampled material is placed between two electrodes. A sinusoidal alternating voltage (U_0) is applied with a fixed frequency $\omega/2\pi$. The resulting current (I_0) is measured, which is related to U_0 tough the frequency dependent impedance.

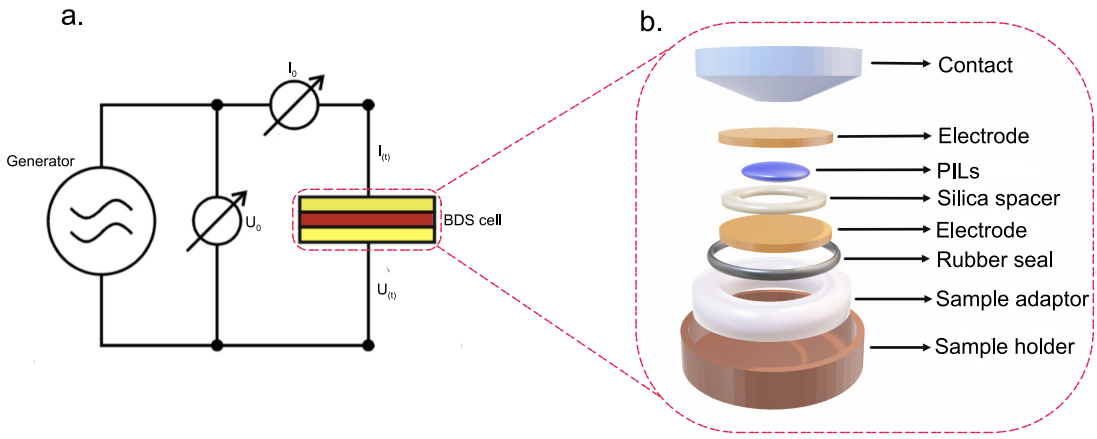

Figure 3.9: Schematic figure for a Broadband Dielectric Spectroscopy (BDS) measurement (a) and the components of the BDS cell used in this thesis (b).

In this thesis, a broadband dielectric spectrometer from Novocontrol GmBh was employed to determine the ionic conductivity of protic ionic liquids. In the case of the alkyl-imidazolium TFSI protic ionic liquids series, the sample was placed in between two identical gold-plated brass electrodes, 13.5 mm in diameter, separated by a 1 mm silica spacer for keeping a precise sample thickness. In the case of triazolium based protic ionic liquids and binary mixture of protic ionic liquids, the samples were sandwiched between 10 mm stainless steel electrodes and separated with a PTFE spacer with an inner diameter of 5 mm and a thickness of 3.1 mm was used, see Figure 3.9b for a representation of a BDS cell. The conductivity measurements were performed

covering the frequency range 10^{-1} - 10^{7} Hz, while the temperature range was varied from -60 to 250 °C in Paper II, and from 20 °C to 140 °C in Paper IV (the temperature cycle also used to analyse the triazolium based ionic liquids), the temperature was controlled using a nitrogen cryostat with a precision of $\pm$0.5 °C, each temperature was stabilized for 600 seconds.

In the case of ionic conductivity measurement of protic ionic liquid-ethylene glycol mixture, Paper I, a CDM 210 conductometry was employed. A standard aqueous solution of KCl (0.01 M) was used for calibration before each measurement. The liquid mixtures were equilibrated for 30 minutes at 30 °C and the temperature precision was $\pm$0.1 °C.

3.5.3 Diffusion NMR

Pulsed-field gradient NMR is useful for measuring the self-diffusion of ionic species in ionic liquids. Pulsed field gradient NMR was theoretically developed and experimentally demonstrated by Stejskal and Tanner and is widely applicable for obtaining self-diffusion coefficient of ionic liquids [57]. A typical experiment to estimate self-diffusion coefficient consist in acquiring spectra at different values of the field gradient, G, or the length of the gradient pulse, δ, while the other parameters are held constant. Then, by plotting the normalised intensity (I/I_0) versus G or δ, the diffusion coefficient obtained by fitting the decay of the signal with the Stejskal-Tanner equation [57]:

$$I = I_0 \cdot exp^{-k} = I_0 \cdot exp - (\gamma \delta G)^2 D(\Delta - \delta/3) \tag{3.9}$$

where I is the signal intensity, I_0 is the signal intensity of spin-echo at zero gradient including T_1 and T_2 terms, D is the self-diffusion coefficient, γ is the gyromagnetic ratio, δ the length of the gradient pulse, and Δ is the diffusion time. The self-diffusion coefficient (D) can be extracted from the slope of the normalised intensity (natural logarithmic scale) versus k.

In this thesis pulsed field gradient NMR experiments were performed on a Bruker Avance 600 spectrometer. In Paper I, the maximum gradient used for each sample was set in the range 200-400 G·cm^{-1}, the pulse duration δ was set to 1 ms, and the diffusion

time was Δ 100 ms. In Paper II, the applied linear gradient was varied in the range 0-550 G·cm^{-1}, the pulse duration δ was set to 2 ms and the diffusion time Δ was 100 ms. The number of acquisitions in each experiment was 32 and the relaxation delay was set to 15 s.

Chapter 4

Results and discussion

4.1 Ionic liquid mixtures

Ionic liquid based mixtures, *i.e.* ionic liquids mixed with a molecular solvent or with another ionic liquid, have recently attracted considerable attention [58–60]. The reasons for investigating such mixtures are various; the most common is to achieve different physicochemical properties than those of the parent compounds, another is to improve one specific property while compromising another less important one, for instance mixing with the purpose of reducing the melting point at the cost of poorer transport and thermal properties. Another interesting aspect of binary mixtures is the overall cost of the resulting material, which in the case of ionic liquids reduces to try minimizing the fraction of the ionic liquid, which is typically the more expensive component.

One main focus in this thesis, has been exploring binary mixtures of protic ionic liquids possibly suitable as proton carriers for use in intermediate temperature PEMFCs. One prerequisite to achieve proton motion is the ability to form an extended hydrogen bonded network, which compounds like water, imidazole, ethylene glycol and protic ionic liquids can fulfill [61, 62]. Therefore, these are the type of compounds that have been considered when preparing the binary mixtures studied in this thesis.

Ethylene glycol (EG) is an organic compound that forms intramolecular and intermolecular hydrogen bonds involving the hydroxyl groups, and has in some cases been studied in mixtures with aprotic ionic liquids [63–67]. Protic ionic liquids, on the other hand, form intrinsic hydrogen bonds that involve the exchangeable proton (typically sitting on the cation) and the oxygen or nitrogen aroms of the anion. To our knowledge, however, binary mixtures based on ethylene glycol and a protic ionic liquid had not been explored before, which gave the opportunity to investigate a new composition, in a wide compositional range. In particular, the intermolecular interactions and the thermal behavior of such mixtures were investigated.

Previous studies on double salt ionic liquids or binary mixtures of ionic liquids indicate that mixing can be a way to reduce the melting point. Nevertheless, most of these studies concerned aprotic, rather than protic, ionic liquids. In the attempt to fill this gap, mixtures of protic ionic liquids solely have been considered in this thesis. Interestingly, an experimental work by Shah Miran and co-workers has shown that keeping the same cation in mixtures of protic ionic liquids could lead to phenomena of proton hopping, which they evidenced by diffusion NMR [68]. In this context, one should consider that compared to the case of neutral molecular compounds, ionic liquid based mixtures present a higher complexity since every ionic liquid comes with one cation and one anion, each with its specific chemical and electronic structure. Hence, with the aim to minimize complexity, the cation was fixed to 1-ethyl-imidazolium $[C_2HIm]^+$ while the anion was varied to be either bistriflimide (also known as bistrifluoroemthylsulfonylimide), $[TFSI]^-$, or triflate, $[TfO]^-$. Our investigation has focused on understanding the interactions established between cations and anions, the changes in the phase behavior, as well as the effects induced to the mechanism of charge transport.

4.1.1 Adding a co-solvent

The pure protic ionic liquid [C_2HIm][TfO] has a melting point at $\approx$ 27 °C [69]. This can be reduced by adding a co-solvent, ideally without sacrificing other properties such as thermal stability or ionic conductivity. Adding water, for example, results in higher ionic conductivity but is not an optimal choice for use in fuel cells operating at tempertaures above 100 °C due to the evaporation of water molecules [70]. As an alternative, water could be replaced by another amphoteric molecular solvent, less volatile yet able to form an hydrogen bonded network. On this line, ethylene glycol was selected as a potentially interesting co-solvent.

Figure 4.1 shows the thermal stability of the mixture based on [C_2HIm][TfO] and ethylene glycol, added at a mole fraction of 0.5. The first decomposition temperature (T_d) of this solution is found at 114 °C, which is lower than for the pure protic ionic liquid, yet making this mixture interesting for applications where the temperature is kept below 100 °C. The analysis of the phase behavior of these mixtures, in the full compositional range and by DSC experiments, shows that the melting point decreases as the mole fraction of ethylene glycol increases, reflecting an interaction between $[C_2HIm]^+$ cations and $[TfO]^-$ anions altered by the presence of ethylene glycol. This effect was further analysed using vibrational spectroscopy.

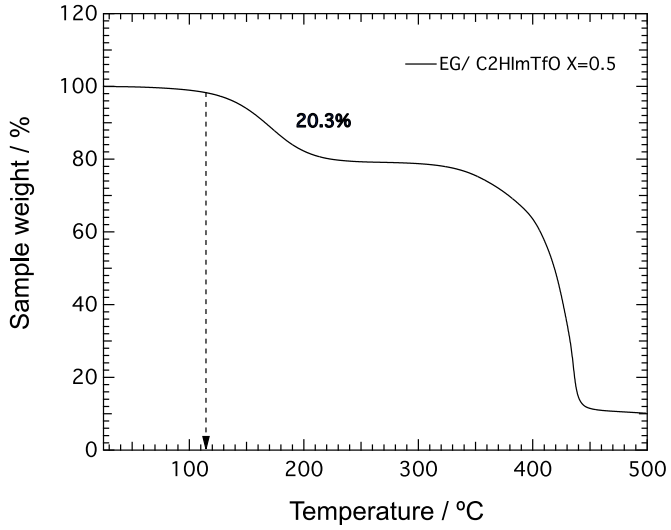

Figure 4.1: Thermal stability, measured by TGA, of a [C_2HIm][TfO] and ethylene glycol mixture, with a mole fraction of ethylene glycol equal to 0.5.

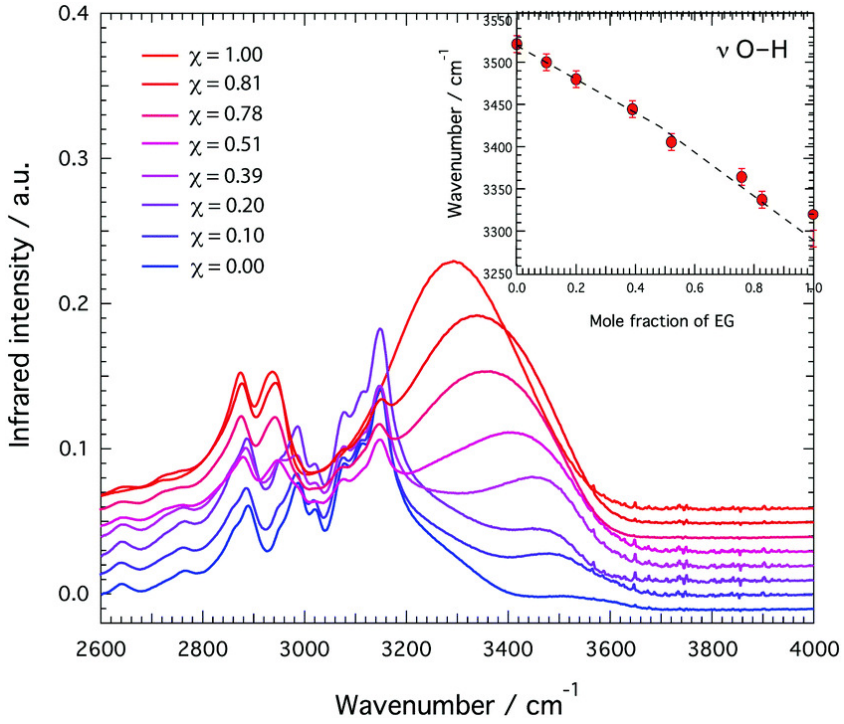

Figure 4.2: Infrared spectra, in the high frequency region, of mixtures based on $[C_2HIm][TfO]$ and ethylene glycol.

The exchangeable proton on the cations of protic ionic liquids is sensitive to changes in its closest molecular environment, which can be caught by infrared spectroscopy. More precisely, in alkyl-imidazolium cations the exchangeable proton is the one on the –NH site, whose N–H stretching mode changes in frequency if the N–H bond length is altered. This could happen, for example, by establishing stronger hydrogen bonds with another proximate molecular species. Figure 4.2 shows the infrared spectra collected for a series of $[C_2HIm][TfO]$-EG binary mixtures (Paper I), in the spectral range 2600 – 4000 cm^{-1}.

The vibrational modes observed between 3200 and 3600 cm^{-1} are associated to N–H stretching mode of the $[C_2HIm][TfO]$ and O–H stretching modes of ethylene glycol. The spectra reveal a clear red shift for the O–H stretching mode, as reproduced in the inset of Figure 4.2. This red shift reflects an elongation of the O–H bond, as a consequence of adding ethylene glycol. This was further supported by NMR spectroscopy, showing that the N(H) proton resonance shifts to higher chemical shift values upon increasing the mole fraction of ethylene glycol in the mixture.

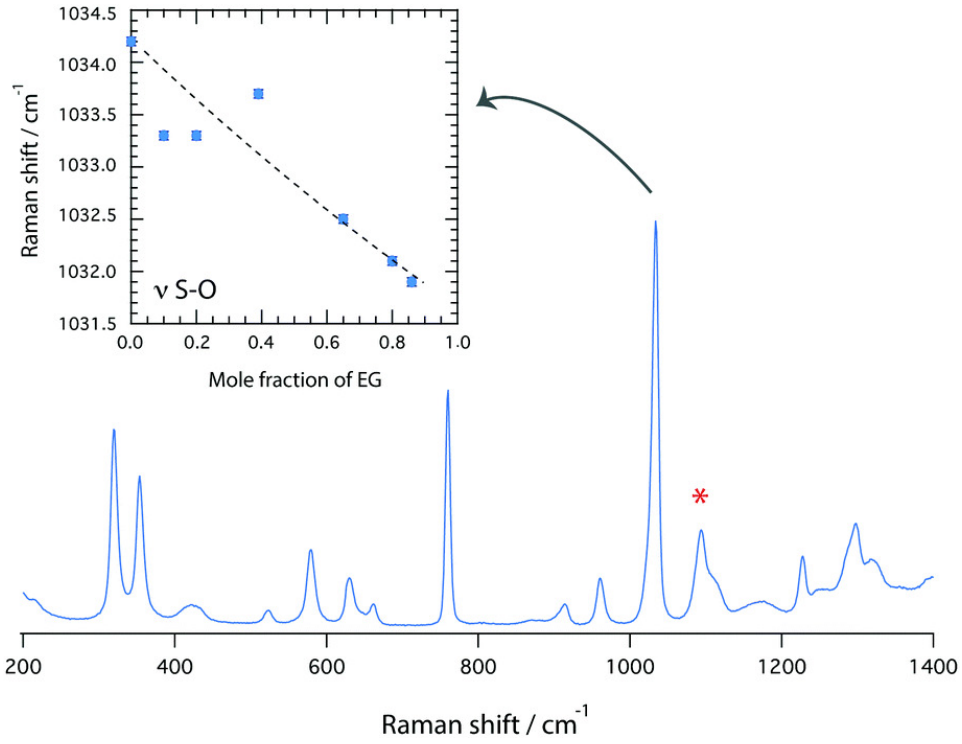

Figure 4.3: A representative result obtained from a Raman spectroscopy experiment for a $[C_2HIm][TfO]$ and ethylene glycol mixture with a mole fraction of ethylene glycol, χ_{EG}, equal to 0.51. The asterisk shows the contribution of ethylene glycol.

The spectroscopic signatures of the anions are better analysed by Raman spectroscopy, that results in distinct and strong peaks associated to $[TfO]^-$, in particular a peak at $\sim$1033 cm^{-1} due to symmetric S–O stretching modes, see Figure 4.3. A careful analysis shows that this mode also red shifts upon addition of ethylene glycol, inset of Figure 4.3. Together, the trends found in Raman and infrared spectra tell that the interaction between $[C_2HIm]^+$ cations and $[TfO]^-$ anions is changed in the presence of ethylene glycol molecules. A local, molecular coordination able to explain these spectroscopic results has been proposed (Paper I).

The diffusivity of the different molecular species present in the mixtures was also found to change with composition. As can bee seen in Figure 4.4, the addition of ethylene glycol results in higher self-diffusion coefficients, D, for all probed species, *i.e.* cations, molecules of ethylene glycol, and the exchangeable protons associated to the -N(H) resonance. In particular, the value od D_{NH} deviates from that of D_{cation}. From these trends it can be concluded that the addition of ethylene glycol affects the

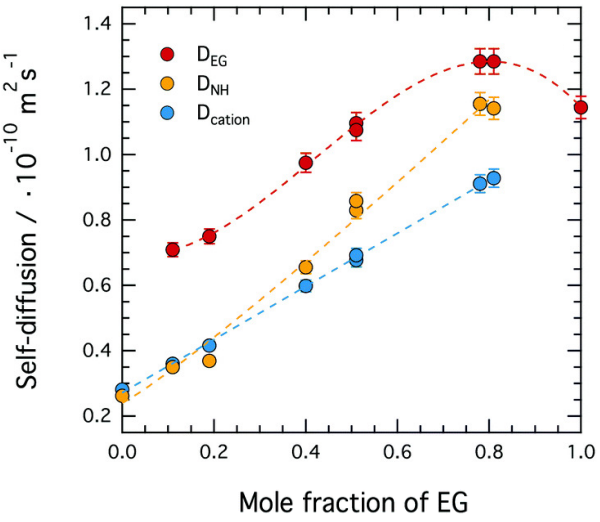

Figure 4.4: Self-diffusion coefficients measured for the exchangeable proton in -NH (D_{NH}), the imidazolium cation (D_{cation}) and ethylene glycol (D_{EG}), as a function of the mole fraction of ethylene glycol in the solution.

cation-anion interaction in a way that reduces viscosity, and that mixing [C_2HIm][TfO] with ethylene glycol promotes proton exchange events that involve the exchangeable protons (since $D_{NH} > D_{cation}$).

The ionic conductivity of these mixtures was evaluated using a CDM conductometer at room temperature, the results being shown in Figure 4.5. The ionic conductivity increases as a function of added ethylene glycol, and reaches a maximum

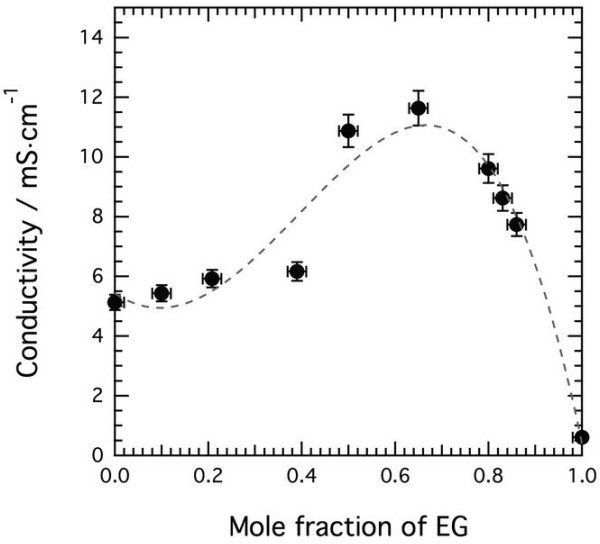

Figure 4.5: Ionic conductivity measured for mixtures of [C_2HIm][TfO] and ethylene glycol (EG), as a function of the mole fraction of ethylene glycol.

value at a mole fraction of ethylene glycol ≈0.6. In absolute values, this increase is less pronounced than for the case of adding water (still to $[C_2HIm][TfO]$), which also shows a bell shaped curve but a maximum at a mole fraction of water closer to 0.9 [61]. This difference is rationalized by the higher viscosity of ethylene glycol (compared to water), hence a weaker effect on the overall ionic mobility. In general, the bell shape as observed in Figure 4.5 can be explained by the co-solvent first contributing positively to the ionic conductivity by dissociating the ions (upwards trend) and then negatively as an effect of a too low concentration of ions (downwards trend) [71–73].

4.1.2 Mixing two protic ionic liquids

Binary mixtures obtained from mixing two (protic or aprotic) ionic liquids have also been the subject of recent research. As an example, Yambou *et al.* [74] and Miran *et al.* [68] have shown important results on the lowering of the melting point and the improvement of the transport properties, when mixing two ionic liquids of the same cation but variable anionic species. These studies where inspirational to the works included in this thesis, which also focused on systems with a fixed and common cation, *i.e.* the protic 1H-ethylimidazolium ($[C_2HIm]^+$) cation, but two different anions, *i.e.* the triflate ($[TfO]^-$) and the bis(trifluoromethylsulfonyl)imide ($[TFSI]^-$).

Figure 4.6 shows the phase behavior, recorded by DSC, of the mixtures based on the two protic ionic liquids $[C_2HIm][TfO]$ and $[C_2HIm][TFSI]$. The figure shows that the solid-to-liquid phase transition, observed as an endothermic peak, is shifted to lower temperatures as the mole fraction of $[C_2HIm][TFSI]$, χ_{TFSI}, in the mixture increases up to 0.2. Also, for values of χ_{TFSI} between 0.3 and 0.8, no endothermic or other peaks were detected, indicating that the liquid state persists over a wide temperature range. This is similar to the phase behaviour observed in mixtures of $[C_2HIm][TFSI]$ and imidazole, for mole fractions of imidazole between 0.17 and 0.8, reported by Yaghini *et al.* [62]. The change in phase behavior as a function of χ_{TFSI} is also a reflection of altered local interactions, that once again were better elucidated by use of vibrational spectroscopy, as discussed below.

Figure 4.7 shows the infrared spectra obtained for the mixtures based on the two

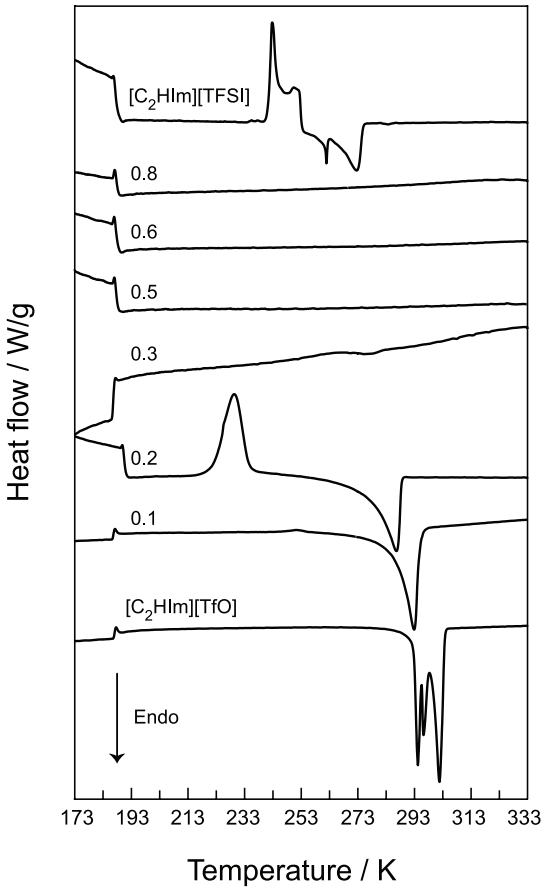

Figure 4.6: Differential scanning calorimetry (DSC) curves recorded during the second heating scan for a series of mixtures based on the protic ionic liquids $[C_2HIm][TfO]$ and $[C_2HIm][TFSI]$. For clarity, the DSC curves have been vertically offset.

protic ionic liquids $[C_2HIm][TFSI]$ and $[C_2HIm][TfO]$ (Paper IV). The N–H stretching mode, found in the frequency range 3200 – 3400 cm^{-1}, is strong and well resolved for pure $[C_2HIm][TFSI]$, but broadens and tends to lower frequencies upon addition of $[C_2HIm][TFO]$. Unfortunately, a more detailed and quantitative analysis of this spectral region was not possible due to the interfering N–H stretching modes arising from $[C_2HIm][TfO]$ (that overlap with those of $[C_2HIm][TFSI]$ and are typically broader and slightly red shifted).

The effect of composition on the state of the anions was better investigated by Raman spectroscopy, as summarized in Figure 4.8. In Figure 4.8a, two characteristic peaks of the anions can be distinguished, *i.e.* the symmetric stretching of the SO_3 group in TfO observed at ca 1033 cm^{-1} and the symmetric stretching of the SO_2 group in TFSI observed at ca 1243 cm^{-1}. These two vibrations change in relative intensity in

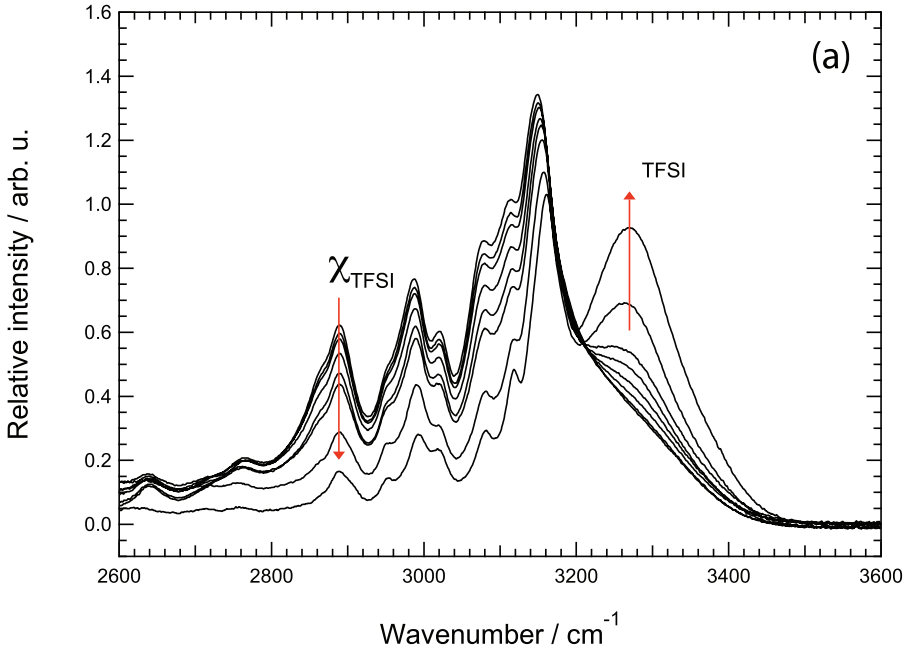

Figure 4.7: Infrared spectra of mixtures of [C_2HIm][TFSI] and [C_2HIm][TfO] in the high frequency spectral range. The arrow indicates the direction of increasing [C_2HIm][TFSI] content.

perfect agreement with the nominal composition of the mixtures. Moreover, by peak fitting the spectral regions around these two vibrations, a precise peak position could be estimated, and plotted as a function of χ_{TFSI}, Figure 4.8b and Figure 4.8c. The vibration related to TfO at ca 1033 cm^{-1} red shifts as χ_{TFSI} increases (Figure 4.8b), and the same is observed for the vibration at ca 1243 cm^{-1} for decreasing values of χ_{TFSI} (Figure 4.8c). These coupled trends indicate weaker anion-cation interactions in the mixtures as compared to the pure protic ionic liquids, and a more disordered ionic system that is congruent with the phase behavior observed by DSC.

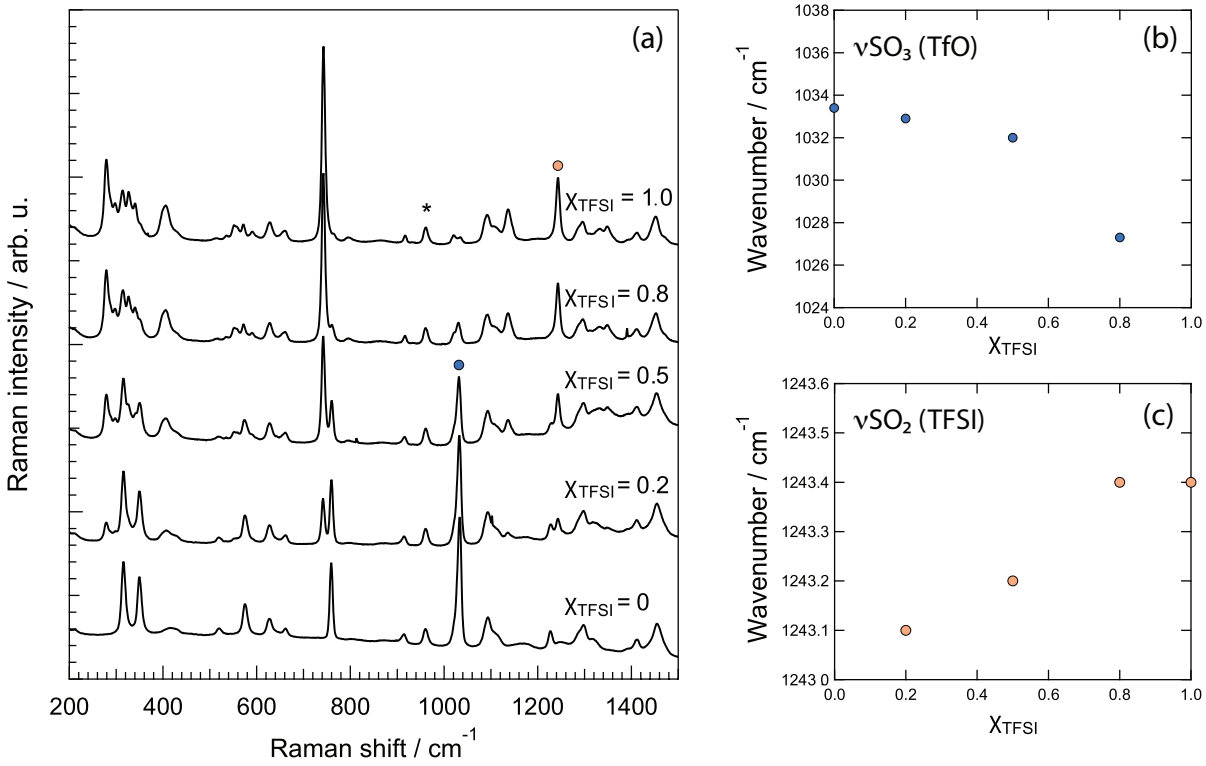

Figure 4.8: Raman spectra of the binary mixtures based on $[C_2HIm][TfO]$ and $[C_2HIm][TFSI]$ in the spectral interval 200–1400 cm^{-1} (a); the spectra have been vertically offset. The frequency of the S–O stretching mode in the TfO and the TFSI anion, as a function of $\chi_{[TFSI]}$, is shown in (b) and (c), respectively.

The ionic conductivity of the binary mixtures of protic ionic liquids was obtained from the frequency-dependent real part of conductivity ($\sigma'(\nu)$), extrapolating from the high-frequency plateau (Paper IV). These conductivity values were then presented in an Arrhenius plot, as shown in Figure 4.9. The ionic conductivity changes only marginally as a function of composition, *i.e.* as χ_{TFSI} increases. This is most likely a direct consequence of the very close ionic conductivity values displayed by the pure ionic liquids mixed, *e.g.* 11.2 mS/cm for pure $[C_2HIm][TfO]$ and 9.9 mS/cm for pure $[C_2HIm][TFSI]$, at 60 °C.

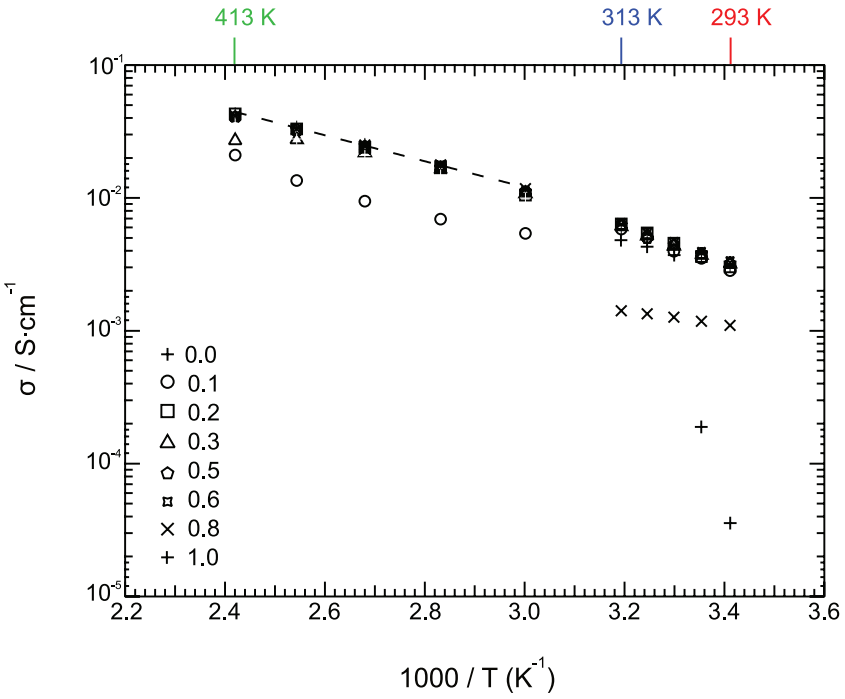

Figure 4.9: Arrhenius plot of the ionic conductivity measured for mixtures of $[C_2HIm][TfO]$ and $[C_2HIm][TTFSI]$.

4.2 Cationic modifications

The structure, size, and symmetry of the cation play a significant role in the resulting properties of the ionic liquid, such as solubility, thermal stability and transport properties [75–79]. A study by Rodrigues *et al.* has shown that the structure of the cation governs the glass transition and melting temperature of aprotic, imidazolium based ionic liquids [80]. Moreover, an investigation by Yoshida *et al.* on imidazolium dicyanamide ionic liquids has revealed significant changes on thermal stability, density, solvatochromic effects, viscosity and ionic conductivity upon modification of the cationic structure [77]. In this thesis, we explored the hypothesis that the thermal and transport properties in imidazolium based protic ionic liquids could be correlated to the nanostructural heterogeneities, that in turn can be tuned by attaching alkyl chains of different length to the cation while keeping the anion fixed (Paper II). Furthermore, whether the thermal and transport properties could be tuned by changing the intrinsic cationic structure, was investigated by synthesizing new protic ionic liquids based on triazolium (Paper III).

4.2.1 Alkyl chains of different length

One important aspect in my studies has been to understand the effect of nanoscale structuration in imidazolium TFSI protic ionic liquids on transport properties and phase behavior. The nanostructural inhomogeneity in ionic liquids (as pure liquids or in mixtures) has been investigated by several techniques, such as SANS and SAXS [40, 81, 82], a pioneering work being that of Russina *et al.* [40] focused on the aprotic ionic liquids 1-alkyl-3-methylimidazolium bis(trifluoromethane)sulfonylimide ([$C_n$mim][TFSI]) with n varying from 2 (ethyl chain) to 10 (decyl chain). These tructural heterogeneities are evidenced by the occurrence of the so called pre-peak in the lower q range (0 – 0.6 Å^{-1}), whose intensity and position is dependent on the length of the alkyl chain attached to the cation. This characteristic peak was also observed in our study, by X-ray scattering, of protic 1-alkyl-imidazolium bis(trifluoromethylsulfonyl)imide ionic liquids, [HC_nIm][TFSI], in which n was varied from 2 (ethyl chain) to 12 (dodecyl chain) (Paper II).

Figure 4.10 shows the WAXS patterns collected for the [HC_nIm][TFSI] series of protic ionic liquids, in which three regions can be distinguished. The first peak (the pre-peak or peak I) appears in the q range 0.2 – 0.6 Å^{-1}, peak II appears in the q range

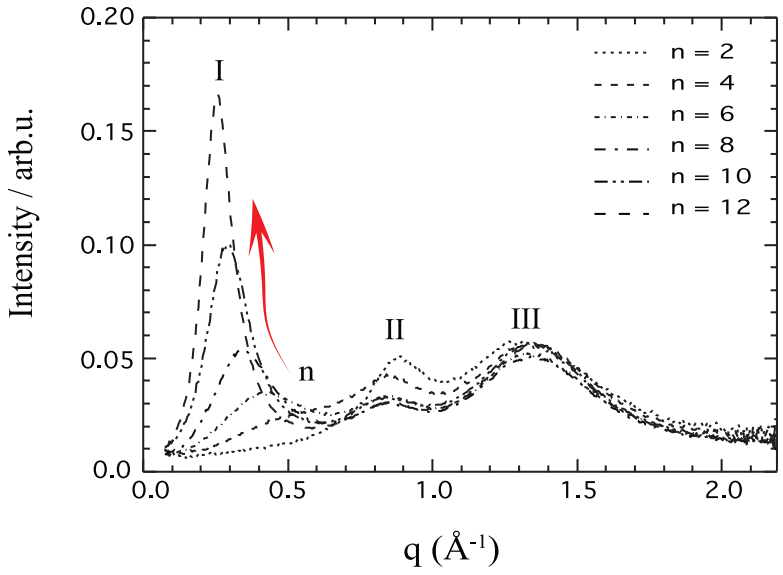

Figure 4.10: Wide-angle X-ray scattering (WAXS) patterns collected for the series of protic ionic liquids [HC_nIm][TFSI], with n varying from 2 (ethyl) to 12 (dodecyl).

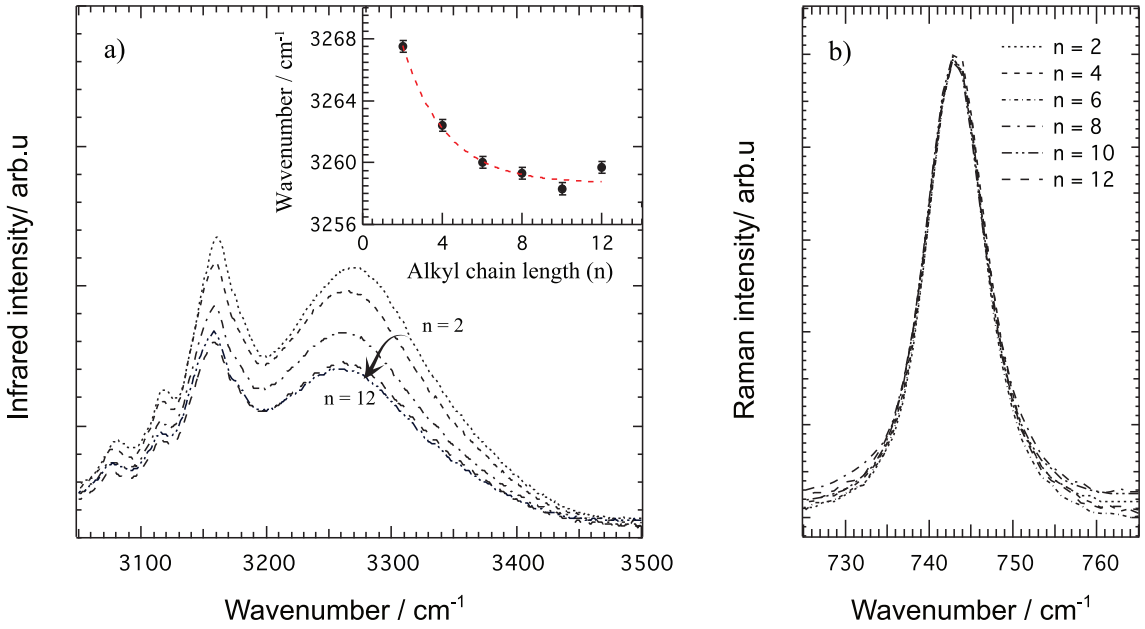

Figure 4.11: Infrared (a) and Raman (b) spectra recorded for the protic ionic liquids in the series [HC_nIm][TFSI]. The frequency dependence of the N–H stretching mode as a function of chain length is shown in the inset of (a), while the Raman spectra show the narrow range 720 – 770 cm^{-1} where the expansion-contraction mode of TFSI appears (b).

0.7 – 0.9 $Å^{-1}$ while peak III apeears in the q range 1.2 – 1.6 $Å^{-1}$. In particular, the intenisty and position of the pre-peak was found to depend strongly on the length of the alkyl chain attached to the cation, a clear sign that nanoscale structuration sets in also in protic ionic liquids (which had not been investigated in this detail before).

To evaluate the correlation between nanostructuration and intermolecular interactions in protic ionic liquids, vibrational spectroscopy was invoked (Paper II). Figure 4.11a shows the infrared spectra of the ionic liquids alkyl-imidazolium TFSI [HC_nIm][TFSI], in the higher frequency region where the N–H stretching modes appear (above 3200 cm^{-1}) that, by virtue of being sensitive to the participation in hydrogen bonds, are of interest in this work. A weak but measurable frequency shift for the N–H stretch was detected, see inset of Figure 4.11a, reflecting the formation of progressively stronger hydrogen bonds as the length of the alkyl chain is increased. For chains longer than the hexyl (n = 6), this frequency change is less pronounced. As a complementary approach, the state of the anions was investigated by Raman spectroscopy, analyzing the spectral range around 743 cm^{-1} where an intense and sharp mode appears

that is assigned to the symmetric bending mode of CF_3 in TFSI. This mode is known to be sensitive to local intermolecular interactions [69]. Interestingly, the Raman spectra collected for these protic ionic liquids do not show any significant dependence on the length of the alkyl chain, Figure 4.11b. These spectroscopic findings are not trivial to rationalize, nevertheless the following scenario has been proposed: for the short chain protic ionic liquids, *e.g.* 1H-ethyl-imidazolium TFSI [HC_2Im][TFSI], the hydrogen bonds that form between the cation and the anion include both the -NH and the ethyl chain on imidazolium, while in the case of longer chains, *e.g.* in [HC_{10}Im][TFSI], the hydrogen bonds are more directional and involve primarily the -NH site of the imidazolium ring. This scenario would be in accordance with the results obtained from WAXS.

From the point of view of thermal stability and phase behaviour, the protic ionic liquids series [HC_nIm][TFSI] was also investigated by TGA and DSC. The thermal stability does not depend significantly on the alkyl chian length, Figure 4.12a, and the decomposition temperature, T_d, stays around 350 °C in all ionic liquids investigated, Figure 4.12b. The mass loss detected up to T_d is larger than expected from the trace amounts of absorbed water, and therefore attributed to proton back transfer events followed by the evaporation of the volatile compounds that form (*i.e.* the pristine acid and base). The phase behavior of these protic ionic liquids revealed an interesting feature,

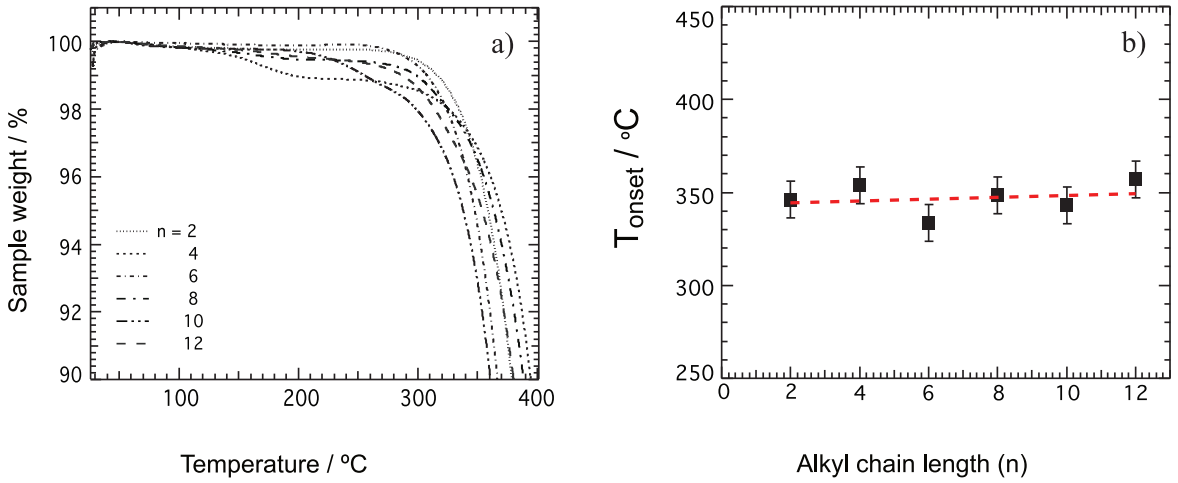

Figure 4.12: Thermogravimetric curves (a) and decomposition temperature, T_d, (b) for all protic ionic liquids in the [HC_nIm][TFSI] series, n varying from 2 (etyl) to 12 (dodecyl).

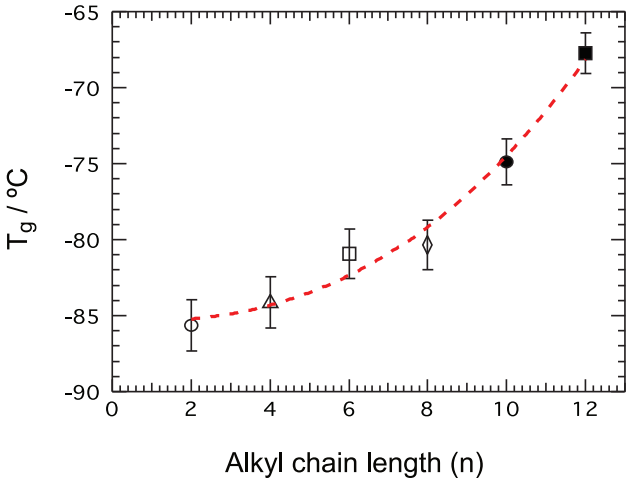

Figure 4.13: Glass transition temperature, T_g, of the protic ionic liquids in the series [HC_nIm][TFSI] as a function of the alkyl chain length, n. The dashed line is simply a guide to the eye.

i.e. for very short (ethyl) and very long (decyl and doddecyl) alkyl chains a distinct solid-to-liquid transition is detected, whilst for intermediate alkyl chains (butyl, hexyl, and octyl) a glass transition only is observed, telling that these ionic liquids are good glass formers. Moreover, the glass transition temperature, T_g, increases monotonically with the length of the alkyl chain, as shown in Figure 4.13. Altogether, the results from these thermal analyses imply that for use in proton exchange membrane fuel cells, the [HC_nIm][TFSI] protic ionic liquids are limited to a temperature of ca 180 °C, an upper limit that is set by the occurrence of proton back transfer events, rather than by decomposition.

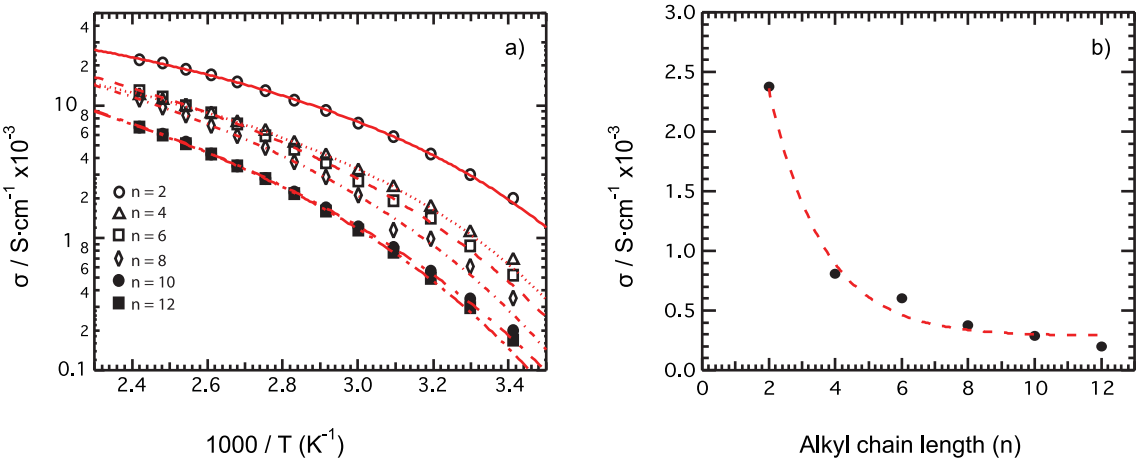

Figure 4.14: a) Arrhenius plot of [HC$_n$Im][TFSI], the data were fit with VFT equation and presented as red lines. b) The ionic conductivity at 25 °C as a function of alkyl chain length; the dashed line is simply guide to the eye.

The ionic conductivity of the [HC$_n$Im][TFSI] protic ionic liquids was investigated by broadband dielectric spectroscopy, the resulting values being presented in the Arrhenius plot of Figure 4.14a. For all ionic liquids, the ionic conductivity increases with temperature following the Vogel-Fulcher-Tammann (VFT) behavior (Paper II); the experimental data were fitted using the VFT equation and energies of activation, E_a, could be estimated. We found that E_a increases with the length of the alkyl chain, taking values between 39 meV (n=2, ethyl) and 51 meV (n=12, dodecyl). Moreover, in absolute values the ionic conductivity decreases monotonically with n, as shown in Figure 4.14b, a trend that is congruent with the increase of T_g (hence the increase in viscosity at room temperature) discussed above.

4.2.2 From imidazolium to triazolium

The great majority of studies treating ionic liquids have concerned cations derived from imidazolium, ammonium, phosphonium and pyridinium, while triazolium is an emerging cation that remains the least investigated. The few works available in the literature that involve the triazolium cation have considered aprotic ionic liquids [83–86], while little has been done with triazolium based protic ionic liquids [87, 88]. Moreover, known synthesis protocols for obtaining protic ionic liquids are sometimes, and unfortunately, simplified to 'mixing equimolar amounts of a Brønsted acid with a base'. This theoretically simple procedure is, in reality, more complicated and limited by several factors such as purity of the reagents, synthesis conditions and viable purification processes. In this context, we have contributed by developing a detailed procedure and protocol for the synthesis of pure and dry protic ionic liquids, including the imidazolium and the triazolium cations in a single comparative work. Our results are likely to pave the way for a new scientific direction, and will guide the interested sceintist in synthesizing a generation of new protic ionic liquids.

More precisely, the base 1,2,4-triazole was reacted with iodoethane in a basic solution to obtain 1-ethyl-1,2,4-triazole. This intermediate product was then reacted without using any solvent with a Brønsted acid with a strong pKa, *i.e.* tri-

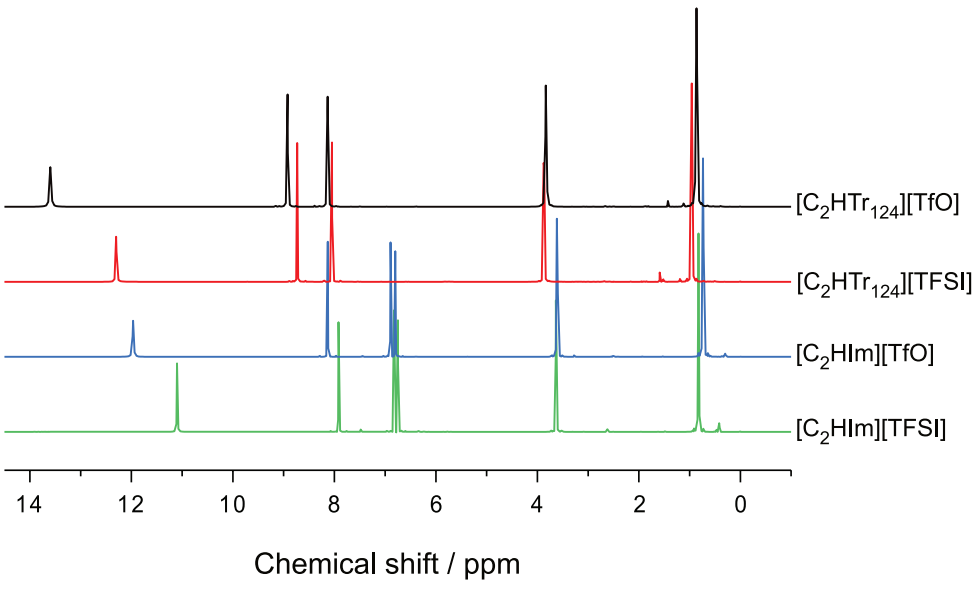

Figure 4.15: ^{1}H NMR spectra of the protic ionic liquids investigated in Paper III.

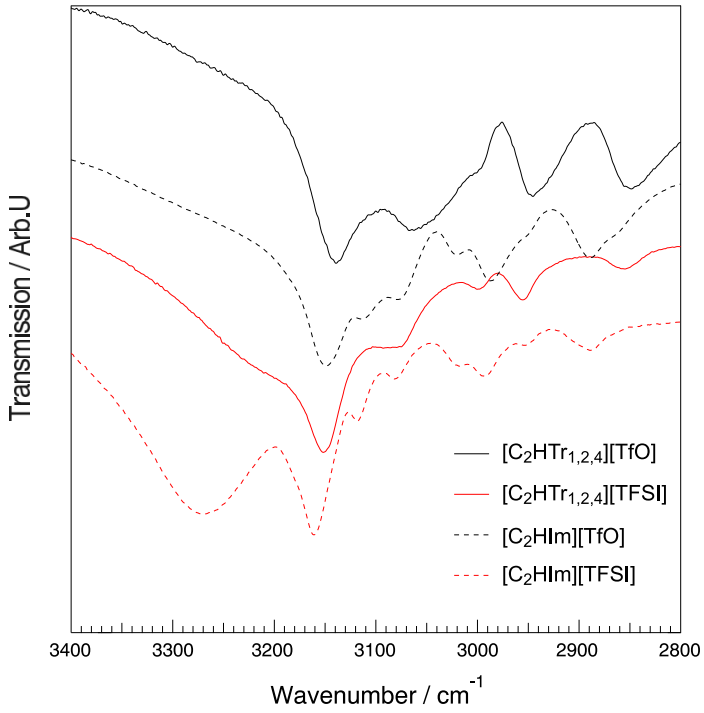

Figure 4.16: Infrared spectra of the four imidazolium and triazolium based protic ionic liquids in the high frequency region where the N–H stretching modes commonly appear.

flic acid (HTfO) and bistriflimide acid (HTFSI), to obtain the protic ionic liquids 1-ethyl-1,2,4-triazolium triflate $[C_2HTr_{1,2,4}][TfO]$ and 1-ethyl-1,2,4-triazolium bistriflimide $[C_2HTr_{1,2,4}][TFSI]$ (Paper III). The chemical characterisation of these compounds was carried out by means of NMR and vibrational spectroscopy, benchmarking to their analogous based on imidazolium, *i.e.*, 1-ethyl-imidazolium triflate $[C_2HIm][TfO]$ and 1-ethyl-imidazolium bistriflimide $[C_2HIm][TFSI]$. The chemical shift of the N-H resonance in ionic liquids commonly appears at high ppm values, typically above 9 ppm, see Figure 4.15. Based on the region where the chemical shift of N-H is found, in this study between 10 and 14 ppm, it is concluded that the triazolium based protic ionic liquids have a more acidic character than those based on imidazolium. Moreover, the anion also has an effect, the $[TfO]^-$ based ionic liquids displaying a ^1H resonance shifted downfield if compared to the case of $[TFSI]^-$, reflecting an enhanced acidity.

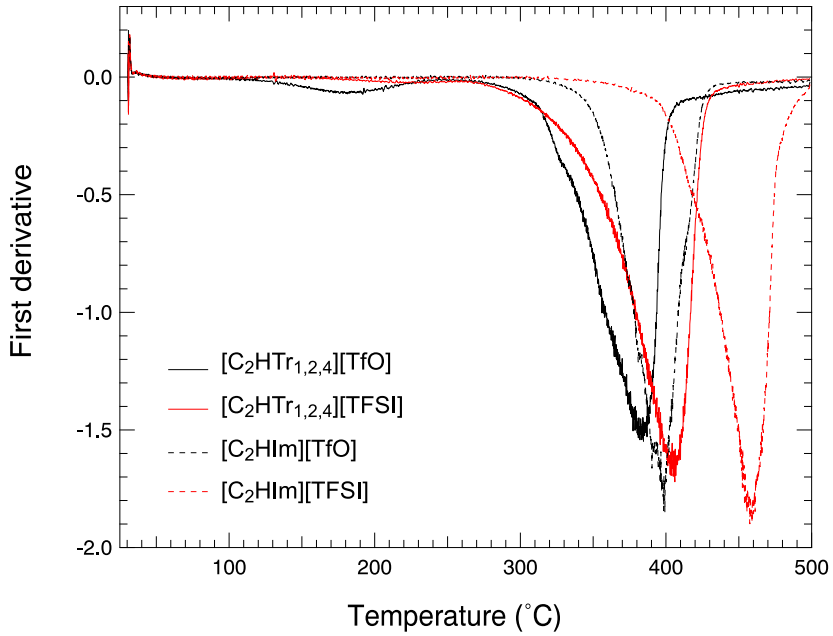

Figure 4.17: The first derivative thermogravimetric analysis results of non heat treated protic ionic liquids.

These trends were also confirmed by infrared spectroscopy, in the high frequency region 3200 – 3300 cm^{-1} where the N–H stretching modes appear, Figure 4.16. This figure reveals a systematic red shift for the N–H stretching mode, with $[C_2HTr_{1,2,4}][TfO]$ displaying the lowest wavenumber and hence the most elongated N–H bonds, *i.e.* a more acidic character. These results are also in agreement with the thermal stability, Figure 4.17, since the triazolium based protic ionic liquid $[C_2HTr_{1,2,4}][TfO]$, for example, shows the lowest temperature DTG peak in the series (*i.e.* at 181 °C) reflecting an ease for proton back transfer events.

The ionic conductivity of these ionic liquids was determined using broadband dielectric spectroscopy (BDS), and are shown in the Arrhenius plot of Figure 4.18. To note, that these ionic conductivity values were measured for temperatures at which all protic ionic liquids are in the liquids state, *i.e.* above 30 °C. The trend among these samples is clear, the triazolium based protic ionic liquids group together and show a slightly lower conductivity than their imidazolium counterparts, while ionic liquids based on the [TfO] anion systematically display a slightly higher conductivity than those based on [TFSI].

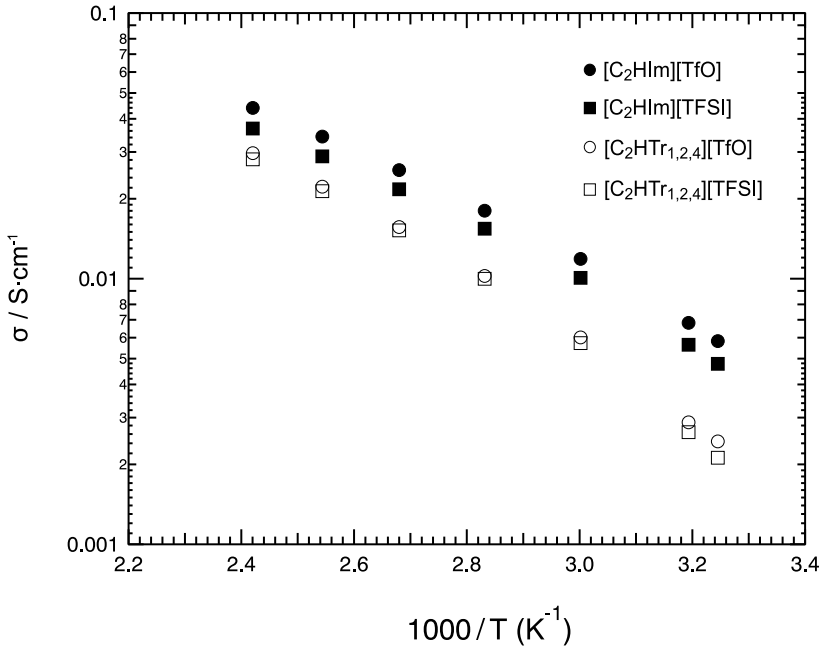

Figure 4.18: Arrhenius plot for the ionic conductivity of $[C_2HTr_{1,2,4}][TfO]$, $[C_2HTr_{1,2,4}][TFSI]$, $[C_2HIm][TfO]$, and $[C_2HIm][TFSI]$.

A net distinction between triazolium based and imidazolium based ionic liquids is also observed from the measured self-diffusion values (preliminary NMR results, yet not published). For the same anion, the triazolium protic ionic liquids display about half the diffusion value of the imidazolium counterpart, see Table 4.1. This reflects the behavior observed for ionic conductivity and indicates that charge is primarily transported by the vehicular mechanism. The latter is further confirmed by the similar values found for D_{cation} and D_{NH}, for all four protic ionic liquids investigated.

Protic ionic liquid	**D_{cation}** ($\cdot 10^{-11}$ $m^2 \cdot s^{-1}$)	**D_{NH}** ($\cdot 10^{-11}$ $m^2 \cdot s^{-1}$)
$[C_2HTr_{1,2,4}][TfO]$	1.199	1.203
$[C_2HTr_{1,2,4}][TFSI]$	1.303	1.412
$[C_2HIm][TfO]$	2.784	2.781
$[C_2HIm][TFSI]$	2.904	2.883

Table 4.1: Self-diffusion coefficients estimated by PFG NMR at 35 °C.

Chapter 5

Conclusions and future outlook

All the results obtained from the first strategy, mixing the ionic liquid with ethylene glycol or another protic ionic liquid, can be summarized as follows. Adding a co-solvent or an ionic liquid has a significant effect on the phase behaviour, primarily reducing the melting point. This results in wider temperature ranges of the liquid state. Furthermore, for some mixed compositions, liquid-to-solid transitions are entirely suppressed, implying further extension of the liquid state window towards extremely low temperatures. These are positive effects, certainly relevant for uses in PEMFCs. Another aspect to consider is the effect of mixing on the transport properties. The ionic conductivity, for instance, can be increased by adding ethylene glycol, albeit only up to a limited mole fraction. By mixing the two protic ionic liquids considered in this work, however, the enhancement in ionic conductivity is less evident, and attributed to the very proximate values of the pure liquids mixed. In both cases, the increased conductivity values measured upon mixing can be explained by an increased local disorder as well as weaker cation-anion interactions. Moreover, upon addition of ethylene glycol indications of a decoupled proton motion are observed, while the same could not be verified for the ionic liquid mixtures.

As for the second strategy, the modification of the imidazolium cation by attaching longer alkyl chains resulted in interesting effects. First of all, it was evidenced that, resembling the case of aprotic ionic liquids, the protic ionic liquids of the alkylimidazolium bistriflimide series, [CnHIm][TFSI], also form distinct nanostructures,

which was revealed by wide angle X-ray scattering (WAXS) experiments. In turn, this nanostructuration influences other properties, *e.g.* it increases T_g, it decreases the ionic conductivity and most importantly, for intermediate chain lengths these protic ionic liquids behave as good glass forming liquids. It must also be noted that none of these protic ionic liquids displayed dynamics that indicate a self-diffusion of the proton faster than that of the parent molecules, in line with the results reported in previous studies performed in our group and available in the literature [62, 89]. In other words, the addition of a base, resulting in non-stoichiometric compositions, is necessary to promote a faster proton motion. Finally, new triazolium based protic ionic liquids were prepared following an own developed synthesis method. This was a tedious work, that finally resulted in highly pure and dry protic ionic liquids based on a truly equimolar ratio between the Brønsted acid and base. I sincerely believe that the developed synthesis protocol will have an impact on the field, since it is reproducible, and easily adaptable to any other laboratory scale research activity. General trends are observed from this work, in particular the higher acidic character of triazolium based protic ionic liquids, compared to the imidazolium counterparts. Also, the interaction between the TFO anion with both the triazolium and the imidazolium cation is stronger than that of TFSI, resulting in longer N–H bonds. This comes, unfortunately, at the cost of a lower thermal stability, since proton back transfer events become easier. As a result of the specific cation-anion interactions, triazolium based protic ionic liquids have lower ionic conductivity and self-diffusivity than those based on imidazolium.

The results from this study can inspire further works related to the symmetry of the triazolium cation. The base triazole exists as two isomers; 1,2,4-triazole and 1,2,3-triazole. As can be judged from the conductivity results, the more symmetric cation leads to a higher ionic conductivity, in this case the 1-ethyl-imidazolium cation. Therefore, a thorough future study could be carried out to investigate the relation between the symmetry in triazolium based protic ionic liquids and their transport properties. Another valuable outlook could be investigating pure or binary systems of the triazolium series upon incorporation in a solid matrix and under real fuel cell operating conditions. For instance, these liquid systems could be integrated into a polymer mem-

brane like Nafion or a cellulose based film [90]. Indeed, demonstrating the use of these or other protic ionic liquids in real fuel cells will be pivotal for further progresses in the direction of PEM materials functional at anhydrous conditions. Finally, triazolium based protic ionic liquids could be mixed with an appropriate base, namely trizole, in order to provide the necessary hydrogen donor-acceptor sites that can assist a fast proton motion, similarly to the behaviour previously observed for imidazole-doped imidazolium based ionic liquids. Mixtures of protic ionic liquids based on the imidazolium and the triazolium cation would also be an ultimate study, mainly from the point of view of phase behaviour and suppressed solid-liquid transitions, with positive implications on the ionic mobilities.

Bibliography

[1] J. Dupont, *Accounts of Chemical Research* **2011**, *44*, 1223–1231.

[2] P. Hapiot, C. Lagrost, *Chemical Reviews* **2008**, *108*, 2238–2264.

[3] J. S. Wilkes, *Green Chemistry* **2002**, *4*, 73–80.

[4] S. K. Nandwani, N. I. Malek, M. Chakraborty, S. Gupta, *Energy & Fuels* **2020**, *34*, 6544–6557.

[5] Z. Lei, B. Chen, Y.-M. Koo, D. R. MacFarlane, *Chemical Reviews* **2017**, *117*, 6633–6635.

[6] Y. Wang, D. F. Ruiz Diaz, K. S. Chen, Z. Wang, X. C. Adroher, *Materials Today* **2020**, *32*, 178–203.

[7] A. Chandan, M. Hattenberger, A. El-kharouf, S. Du, A. Dhir, V. Self, B. G. Pollet, A. Ingram, W. Bujalski, *Journal of Power Sources* **2013**, *231*, 264–278.

[8] C. Austen Angell, Y. Ansari, Z. Zhao, *Faraday Discussions* **2012**, *154*, 9–27.

[9] T. Welton, *Biophysical reviews* **2018**, *10*, 691–706.

[10] J. T. Yoke, J. F. Weiss, G. Tollin, *Inorganic Chemistry* **1963**, *2*, 1210–1216.

[11] J. S. Wilkes, J. A. Levisky, R. A. Wilson, C. L. Hussey, *Inorganic Chemistry* **1982**, *21*, 1263–1264.

[12] J. S. Wilkes, M. J. Zaworotko, *Journal of the Chemical Society Chemical Communications* **1992**, 965–967.

[13] N. V. Plechkova, K. R. Seddon, *Chemical Society Reviews* **2008**, *37*, 123–150.

[14] H. K. Timken, H. Luo, B.-K. Chang, E. Carter, M. Cole in *Commercial Applications of Ionic Liquids*, (Ed.: M. B. Shiflett), Springer International Publishing, Cham, **2020**, pp. 33–47.

[15] M. Abai, M. P. Atkins, A. Hassan, J. D. Holbrey, Y. Kuah, P. Nockemann, A. A. Oliferenko, N. V. Plechkova, S. Rafeen, A. A. Rahman, R. Ramli, S. M. Shariff, K. R. Seddon, G. Srinivasan, Y. Zou, *Dalton Trans.* **2015**, *44*, 8617–8624.

[16] M. Armand, F. Endres, D. R. MacFarlane, H. Ohno, B. Scrosati, *Nature Materials.* **2009**, *8*, 621–629.

[17] M. Galiński, A. Lewandowski, I. Stępniak, *Electrochimica Acta* **2006**, *51*, 5567–5580.

[18] D. R. MacFarlane, N. Tachikawa, M. Forsyth, J. M. Pringle, P. C. Howlett, G. D. Elliott, J. H. Davis, M. Watanabe, P. Simon, C. A. Angell, *Energy & Environmental Science* **2014**, *7*, 232–250.

[19] A. Balducci, *Topic in Current Chemistry.* **2017**, *375*, DOI 10.1007/s41061-017-0109-8.

[20] T. Yasuda, S.-i. Nakamura, Y. Honda, K. Kinugawa, S.-Y. Lee, M. Watanabe, *ACS Applied Materials & Interfaces* **2012**, *4*, 1783–1790.

[21] M. Salanne, *Topic in Current Chemistry.* **2017**, *375*, DOI 10.1007/s41061-017-0150-7.

[22] R. P. O'Hayre, *Fuel cell fundamentals.* Wiley, **2009**.

[23] C. Chiappe, A. Mezzetta, C. S. Pomelli, M. Puccini, M. Seggiani, *Organic Process Research & Development* **2016**, *20*, 2080–2084.

[24] T. L. Greaves, C. J. Drummond, *Chemical Reviews* **2008**, *108*, 206–237.

[25] M. B. Herath, T. Hickman, S. E. Creager, D. D. DesMarteau, *Journal of Fluorine Chemistry* **2011**, *132*, 52–56.

[26] M. Yoshizawa, W. Xu, C. A. Angell, *Journal of the American Chemical Society* **2003**, *125*, 15411–15419.

[27] C. Maton, N. De Vos, C. V. Stevens, *Chemical Society Reviews* **2013**, *42*, 5963–5977.

[28] Y. Chen, T. Mu in *Encyclopedia of Ionic Liquids*, (Ed.: S. Zhang), Springer Singapore, Singapore, **2019**, pp. 1–13.

[29] M. Kohagen, M. Brehm, Y. Lingscheid, R. Giernoth, J. Sangoro, F. Kremer, S. Naumov, C. Iacob, J. Kärger, R. Valiullin, B. Kirchner, *The Journal of Physical Chemistry B* **2011**, *115*, 15280–15288.

[30] N. Yaghini, L. Nordstierna, A. Martinelli, *Physical Chemistry Chemical Physics* **2014**, *16*, 9266–9275.

[31] P. A. Hunt, C. R. Ashworth, R. P. Matthews, *Chemical Society Reviews* **2015**, *44*, 1257–1288.

[32] P. A. Hunt, *Topics in Current Chemistry* **2017**, *375*, 59.

[33] H. Watanabe, H. Doi, S. Saito, M. Matsugami, K. Fujii, R. Kanzaki, Y. Kameda, Y. Umebayashi, *Journal of Molecular Liquids* **2016**, *217*, 35–42.

[34] M. S. Miran, H. Kinoshita, T. Yasuda, M. A. B. H. Susan, M. Watanabe, *Chem. Commun.* **2011**, *47*, 12676–12678.

[35] K. Fumino, A. Wulf, R. Ludwig, *Phys. Chem. Chem. Phys.* **2009**, *11*, 8790–8794.

[36] R. Hayes, S. Imberti, G. G. Warr, R. Atkin, *Angewandte Chemie International Edition* **2013**, *52*, 4623–4627.

[37] M. Campetella, A. Le Donne, M. Daniele, L. Gontrani, S. Lupi, E. Bodo, F. Leonelli, *The Journal of Physical Chemistry B* **2018**, *122*, 2635–2645.

[38] R. Hayes, G. G. Warr, R. Atkin, *Chemical Reviews* **2015**, *115*, 6357–6426.

[39] T. L. Greaves, C. J. Drummond, *Chemical Society Reviews* **2013**, *42*, 1096–1120.

[40] O. Russina, A. Triolo, L. Gontrani, R. Caminiti, D. Xiao, L. G. Hines Jr, R. A. Bartsch, E. L. Quitevis, N. Pleckhova, K. R. Seddon, **2009**, *21*, 424121.

[41] T. L. Greaves, A. Weerawardena, C. Fong, I. Krodkiewska, C. J. Drummond, *The Journal of Physical Chemistry B* **2006**, *110*, 22479–22487.

[42] K.-D. Kreuer, *Chemistry of Materials* **1996**, *8*, 610–641.

[43] P. Ramaswamy, N. E. Wong, G. K. H. Shimizu, *Chem. Soc. Rev.* **2014**, *43*, 5913–5932.

[44] A. Noda, M. A. B. H. Susan, K. Kudo, S. Mitsushima, K. Hayamizu, M. Watanabe, *The Journal of Physical Chemistry B* **2003**, *107*, 4024–4033.

[45] R. Bottom in *Principles and Applications of Thermal Analysis*, John Wiley Sons, Ltd, **2008**, Chapter 3, pp. 87–118.

[46] M. Wagner in *Thermal Analysis in Practice - Fundamental Aspects*, Hanser Publishers.

[47] P. Gabbott in *Principles and Applications of Thermal Analysis*, John Wiley Sons, Ltd, **2008**, Chapter 1, pp. 1–50.

[48] L. Peter, *Infrared and Raman Spectroscopy : Principles and Spectral Interpretation. Vol. Second edition*, Elsevier, **2018**.

[49] G. de, C. Esteves A. Catarina, J. van der Ven Leendert G., M. van Benthem Rolf A. T., J. Laven, R. Tuinier in *Polymer Coatings - A Guide to Chemistry, Characterization, and Selected Applications*, John Wiley Sons, **2019**.

[50] G. Carrillo-Cedillo Eugenia, A. Rodríguez-Avila José, C. Arredondo-Soto Karina, M. Cornejo-Bravo José in *Design of Experiments for Chemical, Pharmaceutical, Food, and Industrial Applications*, IGI Global, **2020**.

[51] S. Mahajan, I. P. Singh, *Magnetic Resonance in Chemistry* **2013**, *51*, 76–81.

[52] A. A. J. Torriero, *Electrochemistry in Ionic Liquids. [electronic resource] : Volume 1: Fundamentals.* Springer International Publishing, **2015**.

[53] A. G. Kikhney, D. I. Svergun, *FEBS Letters* **2015**, *589*, 2570–2577.

[54] N. Osswald, Tim Rudolph in, Hanser Publishers, **2015**, Chapter 1.2.

[55] K. Walters, W. Jones in *Instrumentation Reference Book (Fourth Edition)*, (Ed.: W. Boyes), Butterworth-Heinemann, Boston, **2010**, pp. 69–75.

[56] A. Y. Malkin, A. Isayev in *Rheology - Concept, Methods, and Applications*, 3rd Edition, ChemTec Publishing, **2017**, pp. 265–375.

[57] E. O. Stejskal, J. E. Tanner, *The Journal of Chemical Physics* **1965**, *42*, 288–292.

[58] H. Niedermeyer, J. P. Hallett, I. J. Villar-Garcia, P. A. Hunt, T. Welton, *Chem. Soc. Rev.* **2012**, *41*, 7780–7802.

[59] G. Chatel, J. F. B. Pereira, V. Debbeti, H. Wang, R. D. Rogers, *Green Chem.* **2014**, *16*, 2051–2083.

[60] B. Docampo-Álvarez, V. Gómez-González, T. Méndez-Morales, J. R. Rodríguez, O. Cabeza, M. Turmine, L. J. Gallego, L. M. Varela, *Phys. Chem. Chem. Phys.* **2018**, *20*, 9938–9949.

[61] N. Yaghini, L. Nordstierna, A. Martinelli, *Phys. Chem. Chem. Phys.* **2014**, *16*, 9266–9275.

[62] N. Yaghini, V. Gómez-González, L. M. Varela, A. Martinelli, *Phys. Chem. Chem. Phys.* **2016**, *18*, 23195–23206.

[63] V. Crupi, M. Jannelli, S. Magazu', G. Maisano, D. Majolino, P. Migliardo, D. Sirna, *Molecular Physics* **1995**, *84*, 645–652.

[64] B. Kumar, T. Singh, K. S. Rao, A. Pal, A. Kumar, *The Journal of Chemical Thermodynamics* **2012**, *44*, 121–127.

[65] O. Ciocirlan, O. Croitoru, O. Iulian, *Journal of Chemical & Engineering Data* **2014**, *59*, 1165–1174.

[66] A. Mariani, M. Campetella, C. Fasolato, M. Daniele, F. Capitani, L. Bencivenni, P. Postorino, S. Lupi, R. Caminiti, L. Gontrani, *Journal of Molecular Liquids* **2017**, *226*, Molecular Liquids Meet Ionic Liquids: From Fundamentals to Applications with Particular Attention to Ionic Liquids, 2–8.

[67] A. Gutiérrez, M. Atilhan, R. Alcalde, J. Trenzado, S. Aparicio, *Journal of Molecular Liquids* **2018**, *255*, 199–207.

[68] M. S. Miran, T. Yasuda, M. A. B. H. Susan, K. Dokko, M. Watanabe, *The Journal of Physical Chemistry C* **2014**, *118*, 27631–27639.

[69] N. Yaghini, J. Pitawala, A. Matic, A. Martinelli, *The Journal of Physical Chemistry B* **2015**, *119*, 1611–1622.

[70] N. Yaghini, M. N. Garaga, A. Martinelli, *Fuel Cells* **2016**, *16*, 46–54.

[71] E. Rilo, J. Vila, S. Garcıa-Garabal, L. M. Varela, O. Cabeza, *The Journal of Physical Chemistry B* **2013**, *117*, 1411–1418.

[72] J. Vila, P. Ginés, E. Rilo, O. Cabeza, L. Varela, *Fluid Phase Equilibria* **2006**, *247*, 32–39.

[73] J. N. Canongia Lopes, M. F. Costa Gomes, P. Husson, A. A. H. Pádua, L. P. N. Rebelo, S. Sarraute, M. Tariq, *The Journal of Physical Chemistry B* **2011**, *115*, 6088–6099.

[74] E. P. Yambou, B. Gorska, F. Béguin, *Journal of Molecular Liquids* **2020**, *298*, 111959.

[75] K. A. Kurnia, C. M. Neves, M. G. Freire, L. M. Santos, J. A. Coutinho, *Journal of Molecular Liquids* **2015**, *210*, Mesoscopic structure and dynamics in ionic liquids, 264–271.

[76] A. I. M. C. Lobo Ferreira, A. S. M. C. Rodrigues, M. Villas, E. Tojo, L. P. N. Rebelo, L. M. N. B. F. Santos, *ACS Sustainable Chemistry & Engineering* **2019**, *7*, 2989–2997.

[77] Y. Yoshida, O. Baba, C. Larriba, G. Saito, *The Journal of Physical Chemistry B* **2007**, *111*, 12204–12210.

[78] W. Zheng, A. Mohammed, L. G. Hines, D. Xiao, O. J. Martinez, R. A. Bartsch, S. L. Simon, O. Russina, A. Triolo, E. L. Quitevis, *The Journal of Physical Chemistry B* **2011**, *115*, 6572–6584.

[79] E. A. Arkhipova, A. S. Ivanov, K. I. Maslakov, S. V. Savilov, V. V. Lunin, *Electrochimica Acta* **2019**, *297*, 842–849.

[80] A. S. M. C. Rodrigues, L. M. N. B. F. Santos, *ChemPhysChem* **2016**, *17*, 1512–1517.

[81] D. Pontoni, J. Haddad, M. Di Michiel, M. Deutsch, *Soft Matter* **2017**, *13*, 6947–6955.

[82] L. Almásy, M. Turmine, A. Perera, *The Journal of Physical Chemistry B* **2008**, *112*, 2382–2387.

[83] U. G. Brauer, A. T. De La Hoz, K. M. Miller, *Journal of Molecular Liquids* **2015**, *210*, Mesoscopic structure and dynamics in ionic liquids, 286–292.

[84] L. A. Daily, K. M. Miller, *The Journal of Organic Chemistry* **2013**, *78*, 4196–4201.

[85] A. T. De La Hoz, U. G. Brauer, K. M. Miller, *The Journal of Physical Chemistry B* **2014**, *118*, 9944–9951.

[86] D. Chand, M. Wilk-Kozubek, V. Smetana, A.-V. Mudring, *ACS Sustainable Chemistry & Engineering* **2019**, *7*, 15995–16006.

[87] J. Luo, J. Hu, W. Saak, R. Beckhaus, G. Wittstock, I. F. J. Vankelecom, C. Agert, O. Conrad, *J. Mater. Chem.* **2011**, *21*, 10426–10436.

[88] C. Karlsson, C. Strietzel, H. Huang, M. Sjödin, P. Jannasch, *ACS Applied Energy Materials* **2018**, *1*, 6451–6462.

[89] M. Anouti, J. Jacquemin, P. Porion, *The Journal of Physical Chemistry B* **2012**, *116*, 4228–4238.

[90] O. Danyliv, M. Strach, O. Nechyporchuk, T. Nypelö, A. Martinelli, *ACS Applied Energy Materials* **2021**, *4*, 6474–6485.

Acknowledgements

This research was performed at the division of Applied Chemistry of the Department of Chemistry and Chemical Engineering, also using the facilities at Chalmers Materials Analysis Laboratory, Chalmers University of Technology, and at the Swedish NMR Centre in Gothenburg. This work has been performed by funding support from the Knut & Alice Wallenberg Foundation.

First and foremost, I would like to express my gratitude to my supervisor Prof. Anna Martinelli for giving me the opportunity to work in the field of protic ionic liquids and for all the kind help during my PhD journey, thank you for time whenever I need moral or scientific support. Special thanks to Prof. Jan Swenson for allowing me to learn the beauty of broadband dielectric spectrometer, my examiner Prof. Per-Anders Carlsson, the Directors of studies Prof. Lars Nordstierna and Prof. Nina Kann for always open the door whenever I have questions related to my study.

My gratitude to all collaborators in the appended papers in this thesis.

I am really grateful to all the past and present members of Anna Martinelli's research group: Khalid, Mohammad, Olesia, Szilvia, Eduardo, and Vandna.

Thanks to everyone at the Applied Chemistry division for the enjoyable and welcoming working environment.

I also thank my former supervisor Prof. Lee Ming-Jer, without your introduction to Ionic Liquids world, I would not be where I am today. Also thanks to all previous members in E-504 and *Teknik Reaksi Kimia* laboratory, it has been a pleasure to get to know you all.

I would like to thank all Indonesian friends in Gothenburg. I could not mention all of you but I do appreciate your kind help during my stay in Gothenburg.

Finally, of course, I thank to my family in Indonesia, *Mama, Ayah, Ibu, Bapak, Mbak, Cacak*, Yoga and my lovely wife Eka (*Terimakasih juga untuk kado spesial di penghujung studi S3 ini*).